1 **Genetic dissection of transcription start site selection by RNA Polymerase II in**

2 ***Saccharomyces cerevisiae***

3

4 Payal Arora[1], Kieran F. Brennan[1], Marcie H. Warner[1], Craig D. Kaplan[1]*

5

6 [1]Department of Biological Sciences, University of Pittsburgh, Pittsburgh, Pennsylvania, USA

7 *Address for correspondence: Department of Biological Sciences, University of Pittsburgh,

8 Pittsburgh, PA 15260, Life Science Annex 202, Fifth and Ruskin Avenues, Pittsburgh, PA

9 15260. Email: craig.kaplan@pitt.edu

ABSTRACT

Transcription initiation by RNA Pol II is driven by a preinitiation complex (PIC) comprising Pol II and general transcription factors (GTFs): TFIIA, TFIIB, TFIID, TFIIE, TFIIF and TFIIH. In *Saccharomyces cerevisiae*, transcription start site (TSS) selection proceeds by a promoter scanning mechanism where the PIC scans downstream for TSSs. To determine what factors participate in TSS selection by promoter scanning we designed and implemented forward genetic selections using initiation-sensitive genetic reporters. These reporters were of two types, either being sensitive to upstream or downstream TSS shifts, allowing us to detect alleles that affect promoter scanning in different directions. From >1000 candidates, we identified three primary classes of mutants: existing and novel mutants within known PIC components, including novel alleles of multiple TFIIH subunits; mutants that alter promoter scanning indirectly through cellular conditions (GTP levels and Mn^{2+} levels); and mutants in chromatin and transcription elongation related factors. Genome-wide analysis using TSS mapping shows that tested PIC mutants alter TSS usage globally across promoters while tested chromatin and transcription elongation mutants had much more limited affects. These studies expand the spectrum of mutants able to perturb initiation by promoter scanning and suggest potential plasticity in the TFIIH structure that may be part of the evolution of this initiation mechanism.

INTRODUCTION

Transcription initiation in eukaryotes requires assembly of a large pre-initiation complex (PIC) comprising RNA Polymerase II (Pol II) and general transcription factors (GTF)(CONAWAY AND CONAWAY 1993; ORPHANIDES *et al.* 1996; ROEDER 1996; KORNBERG 2007). Together these components, in conjunction with transcriptional activators and coactivators effect promoter DNA opening, identification of the transcription start site (TSS), and de novo initiation of RNA synthesis using DNA-templated NTP substrates (KAPLAN 2013; ROEDER 2019). Additionally, a large number of other factors are recruited to promoters, including chromatin remodelers and factors functioning in the transition from initiation to elongation (RANDO AND WINSTON 2012). During PIC assembly, TBP and TFIIB bind to the core promoter transiently with TFIIA stabilizing TBP-DNA interactions. Pol II is then recruited to core promoter along with GTFs TFIIF and TFIIE stabilizing the TFIIB-TBP-DNA interactions. Thereafter, TFIIH is recruited into the PIC to drive open complex formation (promoter melting) and subsequent transcription initiation (BAEK *et al.* 2021).

In eukaryotes, the majority of promoters specifies multiple TSSs. In most eukaryotes, a TSS is stereotypically positioned approximately 30-31 basepairs downstream from a site of TBP binding (a canonical TATA-box or otherwise AT-rich sequence) (LIFTON *et al.* 1978; BREATHNACH AND CHAMBON 1981; DUDNYK *et al.* 2024). It is proposed that each TSS is supported by an associated PIC assembly point upstream (KADONAGA 1990; SMALE AND KADONAGA 2003; SANDELIN *et al.* 2007; KADONAGA 2012; VO NGOC *et al.* 2017; LUSE *et al.* 2020; DUDNYK *et al.* 2024). In contrast, transcription initiation in the budding yeast *Saccharomyces cerevisiae* occurs through a promoter scanning mechanism (GIARDINA AND LIS 1993; KUEHNER AND BROW 2006; FAZAL *et al.* 2015; QIU *et al.* 2020). Intriguingly, PIC components and their assembled structure are highly conserved between yeast and humans (BURATOWSKI *et al.* 1988; HE *et al.* 2016; AIBARA *et al.* 2021; SCHILBACH *et al.* 2021; TOMKO *et al.* 2021). While DNA melting by the yeast PIC occurs proximal to its site of binding as in other eukaryotes (GIARDINA

53 AND LIS 1993), the yeast PIC scans downstream for TSSs, which are generally located 40-120
54 bp or further downstream of the TATA box, when present (STRUHL 1987; PARK *et al.* 2014; LU
55 AND LIN 2019; LU AND LIN 2021). TFIIH, required for Pol II promoter DNA opening in all
56 eukaryotes, is proposed to use its DNA translocase activity to continue pumping downstream
57 DNA into the Pol II active site to enable promoter scanning and usage of downstream TSSs
58 (HAMPSEY 2006; MILLER AND HAHN 2006; FAZAL *et al.* 2015; FISHBURN *et al.* 2015).
59 Promoter scanning identifies TSSs based on their inherent sequence characteristics together
60 with the contributions of initiation factor and Pol II activities. Yeast share a universal eukaryotic
61 preference for $Y_{-1}R_{+1}$ as TSSs initiating at a purine (R, representing A or G) and a pyrimidine (Y,
62 representing C or T) at a base upstream with additional species-specific contribution of -8
63 position and contributions of additional bases (HUROWITZ AND BROWN 2003; ZHANG AND
64 DIETRICH 2005; MIURA *et al.* 2006; NAGALAKSHMI *et al.* 2008; ARRIBERE AND GILBERT 2013;
65 PELECHANO *et al.* 2013; MALABAT *et al.* 2015; LU AND LIN 2019; QIU *et al.* 2020; LU AND LIN 2021;
66 ZHU *et al.* 2024). Scanning in yeast was conceptualized by Kuehner and Brow (KUEHNER AND
67 BROW 2006) where TSSs have innate efficiencies of usage, and the alteration of initiation factor
68 activity can alter individual TSS usage and the distribution of TSS usage at promoters (KUEHNER
69 AND BROW 2006; QIU *et al.* 2020; ZHAO *et al.* 2021). Genetic and molecular experiments have
70 shown that TSS selection in yeast is sensitive to mutation in multiple PIC components (*e.g.* Pol
71 II and GTFs (PINTO *et al.* 1992a; PINTO *et al.* 1994; FAITAR *et al.* 2001; GHAZY *et al.* 2004;
72 FREIRE-PICOS *et al.* 2005; KHAPERSKYY *et al.* 2008; JIN AND KAPLAN 2014; QIU *et al.* 2020; ZHAO
73 *et al.* 2021) and PIC-associated components (*e.g.* the conserved factor Sub1, which is the yeast
74 homolog of PC4 (KNAUS *et al.* 1996; WU *et al.* 1999; SIKORSKI *et al.* 2011; BRABERG *et al.* 2013).
75 Mutations in the active site of Pol II that increase Pol II catalytic activity increase efficiency of
76 initiation at each available TSS (KAPLAN *et al.* 2012; JIN AND KAPLAN 2014; QIU *et al.* 2020). With
77 each TSS being more efficient in promoting initiation, the flux of scanning Pol II can be
78 exhausted earlier than WT, leading to an observed upstream shift in observed TSS usage

79 (KUEHNER AND BROW 2006; QIU *et al.* 2020). Similarly, decrease in Pol II catalytic activity causes
80 reduced efficiency of individual TSSs, resulting in increases in the flux of scanning Pol II
81 reaching downstream positions, and an observed downstream shift in TSS usage (KUEHNER
82 AND BROW 2006; QIU *et al.* 2020).

83 In contrast to Pol II, because TFIIH is hypothesized to drive scanning through its Ssl2
84 translocase subunit (FAZAL *et al.* 2015; FISHBURN *et al.* 2015; TOMKO *et al.* 2017; TOMKO *et al.*
85 2021; ZHAO *et al.* 2021), the effects of mutations in Ssl2 on TSS distributions have been
86 interpreted as being due to altered TFIIH processivity (ZHAO *et al.* 2021). *ssl2* alleles that confer
87 downstream shifts to TSS distributions have been interpreted as increasing scanning
88 processivity due to a higher probability of scanning reaching downstream positions. In contrast,
89 *ssl2* alleles that confer upstream shifts to TSS distributions appear to do so by limiting scanning
90 processivity, meaning that downstream positions are reached at a lower probability (KUEHNER
91 AND BROW 2006; ZHAO *et al.* 2021). While TFIIH and Pol II are the primary activities driving TSS
92 selection, how GTFs contribute to either efficiency or processivity pathways or through
93 additional mechanisms is not known (JIN AND KAPLAN 2014; QIU *et al.* 2020).

94 Mutations in other GTFs like TFIIB (PINTO *et al.* 1992a; PINTO *et al.* 1994; BANGUR *et al.*
95 1997; PARDEE *et al.* 1998; FAITAR *et al.* 2001; JIN AND KAPLAN 2014) and TFIIF (SUN AND
96 HAMPSEY 1996; GHAZY *et al.* 2004; JIN AND KAPLAN 2014) also affect TSS distributions, and
97 where tested do so genome wide (QIU *et al.* 2020), as do tested Pol II and *ssl2* alleles of TFIIH
98 (QIU *et al.* 2020; ZHAO *et al.* 2021). Mutations in TFIIB cause downstream shifts to TSS usage in
99 ways that appear consistent with both TFIIB and the Pol II active site determining initiation
100 efficiency at all TSSs (WU *et al.* 1999; FAITAR *et al.* 2001; KOSTREWA *et al.* 2009; JIN AND
101 KAPLAN 2014; QIU *et al.* 2020). Additionally, published mutations in TFIIF, the GTF recruiting Pol
102 II to the core promoter, have also been shown to shift TSSs upstream (SUN AND HAMPSEY 1995;
103 GHAZY *et al.* 2004; FREIRE-PICOS *et al.* 2005; JIN AND KAPLAN 2014; QIU *et al.* 2020). Because
104 specific alleles of TFIIF and TFIIB have been found to mutually suppress each other (GHAZY *et*

105 *al.* 2004; FREIRE-PICOS *et al.* 2005) and also additively interact with Pol II alleles (JIN AND
106 KAPLAN 2014; QIU *et al.* 2020), we have proposed that at least some TFIIF mutants affect TSS
107 selection by functioning alongside the Pol II active site in promoting initiation efficiency (GHAZY
108 *et al.* 2004; FREIRE-PICOS *et al.* 2005; JIN AND KAPLAN 2014) (Jin and Kaplan 2014, Ghazy *et al.*
109 2004; Freire-Picos *et al.* 2005). The interface between Pol II and TFIIH is also important for
110 scanning and has been proposed to be a key factor in the evolution of the scanning mechanism
111 (YANG *et al.* 2022; YANG *et al.* 2024). TFIIH is tethered to the PIC via the RING finger domain of
112 Tfb3 (TFIIK kinase subdomain of TFIIH) through interactions with TFIIE and the Rpb7 subunit of
113 Pol II (SCHILBACH *et al.* 2017; YANG *et al.* 2022; YANG *et al.* 2024). In yeast, mutations in both
114 Rpb7 (BRABERG *et al.* 2013) and Tfb3 (YANG *et al.* 2024) can confer upstream shifts to TSS
115 usage in vivo, consistent with a defective scanning process (Basnet *et al.*; in preparation).
116 Factors outside of PIC such as chromatin and elongation factors have also been implicated to
117 affect promoter choice and potentially TSS selection.
118 PIC factors (Pol II and GTFs) and PIC-associated factors like Sub1 have been
119 genetically identified as contributing to TSS-selection during promoter scanning. What is not
120 known is how many additional factors might also contribute to the process of TSS selection. Are
121 there additional factors that cooperate or contribute to TSS selection but have not been
122 structurally located in the PIC akin to Sub1? What are the surfaces and networks within the PIC
123 that contribute to TSS selection by promoter scanning? Finally, promoter chromatin structure
124 can easily be imagined to affect PIC function and TSS distribution profiles because most yeast
125 promoters have TSSs that map within boundaries of the +1 nucleosome (RANDO AND WINSTON
126 2012). We have aimed to take an unbiased approach to identify any additional factors that
127 participate in TSS selection during initiation by promoter scanning using forward genetic
128 selections (BROW 2019; WANG *et al.* 2025). Through the use of existing (BERROTERAN *et al.*
129 1994) and novel genetic reporters, we have identified ~300 mutations in proteins within and
130 outside the PIC affecting TSS selection, including a number of alleles of Pol II

131 elongation/chromatin genes, *eg. SPT2, SPT4, SPT5, SPT6, SPT16, SPN1, BUR2*, and
132 histones. We then examined a subset of the novel alleles in genetic interaction studies to probe
133 relationships between mutant alleles. Finally, we examined the genome-wide effects of selected
134 PIC and chromatin/elongation-class alleles for effects on TSS-selection. We have found that
135 tested GTF alleles alter TSS usage genome wide as predicted from effects on promoter
136 scanning in general. In contrast, chromatin or Pol II elongation-class alleles did not show similar
137 widespread effects. We interpret this class of mutant as acting on TSSs in a promoter-selective
138 fashion.
139

140 **RESULTS**

141 **TSS-shifting mutants identified by transcription initiation genetic reporters**

142 To understand the genetic requirements for initiation by promoter scanning, we established
143 genetic selection systems for the isolation of transcription start site-shifting mutants. We
144 deployed four initiation reporter alleles designed or chosen because expression from the
145 reporter is sensitive to altered TSS selection: *imd2Δ::HIS3, cyc1-1019::HIS3*, *adhΔ50::HIS3,*
146 and *hmo1Δ38::HIS3* (**Fig. 1**). These reporters comprise native (*imd2Δ::HIS3*) (MALIK *et al.* 2017)
147 or engineered (*cyc1-1019::HIS3*, *adhΔ50::HIS3* and *hmo1Δ38::HIS3)* (FURTER-GRAVES AND
148 HALL 1990; PINTO *et al.* 1992b) promoters have each been fused to the *HIS3* ORF. In wild type
149 cells, they generally do not express sufficient levels of *HIS3* gene product to confer growth on
150 medium lacking histidine (the His^- phenotype). In the presence of a TSS selection mutant
151 conferring an upstream or downstream shift appropriate to the reporter configuration, a shift in
152 TSS usage leads to expression of a functional *HIS3* mRNA, allowing cells to grow on medium
153 lacking histidine (the His^+ phenotype)(**Fig. 1a**). We tuned our phenotypic selections through the
154 use of the drug 3-aminotriazole (3AT), a competitive inhibitor of His3p (KLOPOTOWSKI AND
155 WIATER 1965; STRUHL AND DAVIS 1977), allowing a shift in the threshold of reporter activity
156 needed to confer the His^+ phenotype and beneficial for reporters that allowed leaky *HIS3*

157 expression in WT cells (**Fig. 1b**). We reasoned that using two different promoters for each class
158 of TSS-shift reporter would allow us to prioritize mutants more likely to affect promoter scanning
159 globally as opposed to reporter-specific alleles. We previously developed the *imd2Δ::HIS3*
160 reporter where *HIS3* replaces the *IMD2* ORF and is under control of the *IMD2* promoter (MALIK
161 *et al.* 2017). Downstream shifts to TSS usage bypass a terminator element in the *IMD2*
162 promoter and allow expression of the downstream ORF (KOPCEWICZ *et al.* 2007; JENKS *et al.*
163 2008; KUEHNER AND BROW 2008). We found this reporter exquisitely sensitive to defects in Pol II
164 and GTFs leading to downstream TSS shifts (MALIK *et al.* 2017) and also that we could identify
165 alleles of *SSL2* (ZHAO *et al.* 2021) or *TFA1* and *TFB3* (Basnet et al, in preparation) able to
166 suppress this reporter through genetic screens. Therefore, this reporter appears sensitive to
167 mutations in multiple PIC components that might each alter promoter scanning in distinct ways,
168 *i.e.* controlling Pol II initiation efficiency or controlling scanning processivity.
169 Our other downstream shift-detecting reporter *cyc1-1019::HIS3* functions analogously to
170 *imd2Δ::HIS3* (NA *et al.* 1992; PINTO *et al.* 1992a; PINTO *et al.* 1992b). Here, downstream shifts in
171 TSS usage allow bypass of an introduced upstream ATG (the *cyc1-1019* allele). The introduced
172 ATG allows translation initiation out of frame with *HIS3* and confers a His^- phenotype. Shift to
173 use of downstream TSSs allows translation to begin at the normal *HIS3* ATG. This reporter
174 configuration was used to identify the first *SUA7* (TFIIB) alleles (PINTO *et al.* 1992b) as well as
175 alleles of *RPB1* (*SUA8*) (BERROTERAN *et al.* 1994). This reporter is less leaky than *imd2Δ::HIS3*
176 and thus more tightly His^- even in the absence of 3-AT (**Fig. 1b**). We demonstrated that strong
177 downstream shifting mutants *rpb1* H1085Y and *sub1Δ* were His^+ using this reporter (**Fig. 1b**).
178 Our upstream shifting reporters function analogously to each other. In each case, a reduced
179 TSS to ATG distance likely hampers translation initiation of *HIS3* because the *HIS3* ATG is too
180 close to the 5′ end of the mRNA (FURTER-GRAVES AND HALL 1990). 5′ extension of the mRNA
181 through usage of an upstream TSS allows more efficient *HIS3* translation initiation. We
182 employed *adh50Δ::HIS3*, previously shown to detect *rpb9* alleles as upstream shifters (FURTER-

183 GRAVES AND HALL 1990; FURTER-GRAVES *et al.* 1991), and a second, novel upstream reporter.
184 To create an additional upstream shift-detecting reporter, we analyzed our previous genome
185 wide TSS data (QIU *et al.* 2020) for promoters that showed especially large shifts in TSS usage
186 in response to upstream TSS mutants, settling on *HMO1*. We then fused different lengths of the
187 *HMO1* promoter, truncated by 38, 45 and 53 basepairs to *HIS3* to ask if any of these
188 configurations could cleanly detect upstream TSS-shifting mutants (**Fig. S1a**). First, we tested if
189 these variants could function effectively as potential initiation reporters by assessing if they
190 showed suppressibility when exposed to UV mutagenesis (**Fig. S1a**), an approach previously
191 tested for reporter suppressibility (HAMPSEY 1991). After observing reporter suppressibility, we
192 tested them in conjunction with TSS-shifting Pol II and *rpb9* mutants (**Fig. 1b**).
193
194 **Identification of novel upstream and downstream TSS-shifting mutants**
195 For our selections, we integrated our engineered reporters (*cyc1-1019::HIS3*, *adhΔ50::HIS3* and
196 *hmo1Δ38::HIS3*) at a gene-free locus on chromosome I (**Fig. S1b**) (GRUBER *et al.* 2012) with
197 *imd2Δ::HIS3* present at the native *IMD2* locus. We isolated suppressors of initiation reporters by
198 genetic selection of His^+ candidates and did so in two batches with two versions of genetic
199 selection strains. In an initial pilot genetic selection, ~700 candidates were isolated across the
200 four first generation strains carrying the reporters described above, with the majority isolated
201 from the *IMD2* reporter. Candidates were re-phenotyped for their His^+ phenotypes and for
202 secondary conditional or transcription-related phenotypes. These included growth on YPD at
203 30°C, 16°C, 37°C and with 3% formamide, SC supplemented with MPA to detect MPA
204 sensitivity commonly observed for known upstream shifting TSS alleles (ZHAO *et al.* 2021), SC-
205 Lys medium to test for suppression of the Spt^- reporter allele *lys2-128∂* (SIMCHEN *et al.* 1984;
206 CUI *et al.* 2016), and YPRafGal with YPRaf as a control for suppression of *gal10Δ56* (GREGER
207 AND PROUDFOOT 1998; GREGER *et al.* 2000; KAPLAN *et al.* 2005), a reporter allele able to detect
208 different kinds of transcription-associated phenotypes. We utilized profiles of phenotypes to

209 potentially cluster mutants by similarity of their additional phenotypes and to choose candidates
210 from distinct phenotypic groups for further study. Additionally, known phenotypes of existing
211 mutants allow provisional attribution of candidates to possible candidate genes. We chose 168
212 of these candidates for sequencing using a custom Illumina AmpliSeq amplicon pool (WANG *et*
213 *al.* 2025). Of 168 candidates sequenced using Illumina AmpliSeq, we identified a potential
214 causative mutation in 72 of them. For genes already linked to TSS selection, we identified
215 alleles of *SUA7* (2 unique alleles), *RPB1* (8 unique alleles), *RPB2* (8 alleles from 11
216 candidates), *RPB9* (2 unique alleles), and *SUB1* (3 alleles from 4 candidates). Because of
217 inconsistent coverage with AmpliSeq, we piloted whole genome sequencing for 10 of the initial
218 candidates where AmpliSeq failed to identify a candidate mutation. Whole genome sequencing
219 (WGS) identified potential causative mutations for 7/10 candidates sequenced and provided
220 information allowing refinement of our selection procedures as described below.
221 This preliminary analysis allowed us to refine our selections for a second round where we
222 identified additional both upstream- and downstream-shifting candidates (**Figs. 2, 3, 4, 5**). We
223 identified transcription-related mutants (subset displayed in **Figs. 2, 3, 4, S2, S3**) but also
224 identified classes of mutant that appear reporter specific (*e.g.* guanine metabolism, **Fig. 5a**) and
225 a likely indirect modulator of TSS selection (e.g. *PMR1*, **Fig. 5b**), classes that AmpliSeq would
226 have failed to identify. We then incorporated secondary screening to filter these latter classes
227 out as discussed in the next section. Among upstream-shifting candidates, we filtered out
228 recessive loss of function mutants in *RPB9* by a complementation assay. In a subsequent third
229 round genetic selections we isolated ~1750 more candidates comprising 447 suppressors of
230 *imd2Δ::HIS3*, 672 of *cyc1-1019::HIS3* (**Fig. 2a**), 293 of *adhΔ50::HIS3,* and 350 of
231 *hmo1Δ38::HIS3* (**Fig. 3a**) and after phenotyping-based filtering we prioritized ~250 candidates
232 for whole genome sequencing. In a separate selection of *imd2Δ::HIS3* suppressors performed
233 by the students in the BIOSC 0068 Foundations of Biology Laboratory 2 course at the University
234 of Pittsburgh, 48 His^+ candidates were prioritized by phenotypic and genotypic screens for

235 whole genome sequencing yielding 46 candidates. These were combined with the above 447
236 *imd2Δ::HIS3* suppressor phenotypes above amounting to 495 *imd2Δ::HIS3* suppressors (**Fig.**
237 **2a**). Prioritization across all reporter classes resulted in a total of ~300 candidates sequenced
238 by whole genome sequencing. Out of the ~300 candidates sequenced, we identified reporter
239 transcription-associated mutations in ~240 of these and further ~160 unique mutants.

240 Of all transcription-related mutants isolated in this study, we observed three primary
241 groups: PIC mutants, indirect effectors of TSS selection (*e.g. PMR1*) or promoter specific non-
242 transcription factors *e.g.* guanine mutants), and chromatin/Pol II elongation factors. We
243 validated 8 candidates through reconstruction of mutants by generating alleles in a clean
244 genetic background and all 8 reflected suppressor candidates phenotypically (**Fig. 2b**). In
245 addition to direct validation by reconstruction of a subset of mutants, several lines of evidence
246 support the mutations identified by WGS are causative for phenotypes. First, we selected
247 spontaneous suppressors, so the expectation was for most strains to have essentially a single
248 causative mutation. Second, we identified previous described alleles of *SUA7*, *RPB1*, *RPB2*,
249 *TFB3*, *SPT6*, and *TFA1* while not observing changes elsewhere in their genomes. Third, we
250 identified multiple inactivating alleles of *SUB1* and *RPB9* as expected for non-essential genes
251 with known effects on TSS selection, while not observing changes elsewhere in their genomes.
252 Fourth, there were five cases where we identified the identical allele independently in separate
253 selections. Finally, nearly all candidate sequencing data showed only a single change in gene
254 that could rationally be linked to transcription initiation. Because previous genetic interaction
255 studies have helped annotate functions to mutations (JIN AND KAPLAN 2014; ZHAO *et al.* 2021),
256 we tested inter-subunit interface mutants and genetic interactions across a subset of our
257 mutants before assessing TSS shifts caused by our novel mutants genome wide, which we
258 discuss later.

259 Among mutants in PIC components, we identified alleles of Pol II (*RPO21/RPB1*, *RPB2*,
260 *RPB9*, *RPB10*) and of GTFs (TFIIB, *TFA1*/TFIIE, *TFG2*/TFIIF, TFIIH: *SSL2*, *SSL1*, *TFB2*, *TFB3*,
261 *TFB4* and *RAD3*) (**Fig. 4**). We first observed a high prevalence of mutations in the downstream
262 shifting class lining the activity cleft encompassing *RPB1* and *RPB2*. Because *RPB1* and *RPB2*
263 are larger genes, these mutants predominated in our selections though many of these mutations
264 were novel (**Figs. 4a, b**). Because downstream shifting is expected from reduced Pol II activity
265 (KAPLAN *et al.* 2012; MALIK *et al.* 2017), catalytic or structural defects that lead to reduced
266 catalytic activity or PIC function are expected to be isolated as downstream shifters. However,
267 not all *rpb* mutants clustered around the active site (**Figs. 4a, b**). We observed two types of
268 mutations amongst those surrounding the activity cleft. We found that in both Rpo21/Rpb1 and
269 Rpb2, mutations within structural domains surrounding the cleft displayed formamide sensitivity
270 (**Fig. 4d**), a phenotype that could reflect protein folding or stability defects. Mutations facing or
271 on the surface of the cleft generally were formamide resistant. We also isolated mutations at
272 intra-subunit interfaces including those linked to control Pol II catalysis. For example, we
273 isolated an upstream-shifting mutation G707V in the Rpb1 anchor loop region (**Fig. 4e**). This
274 loop lies between α20 and α21 helices of Rpb1 and (KASTER *et al.* 2016) and a poly-alanine
275 substitution at Rpb1 707-709 in the anchor loop was previously shown to confer MPA sensitivity,
276 consistent with an upstream shift in TSS usage (KASTER *et al.* 2016). We additionally observed
277 mutations in the Rpb1 α21 helix A725T and E734D, both resulting in downstream shifts. A prior
278 mutation in Rpb1 α21, G730D, was identified as a reduced catalytic activity mutant and
279 appeared to function through incompatibility with Rpb9 in that slow growth of G730D was
280 suppressed by rpb9Δ (KASTER *et al.* 2016). It is possible that these substitutions work similarly
281 though they are predicted to be more subtle. Alternatively, E734 is positioned to potentially
282 interact with a network of residues that connects to an Rpb1-Rpb8 interaction but is also
283 adjacent to TFIIS when it is inserted into the active site. However, no role for TFIIS in TSS

284 selection has yet been described. Regardless, perturbation to E734 could result in reduced Pol
285 II catalysis, leading to a downstream shift it TSS usage.
286 Of Rpb2 mutations, beyond the active cleft, we observed mutations in Pol II-lobe-jaw
287 domain along the path of DNA entry near the Rpb9-TFIIF interface (HEMMING *et al.* 2000) (**Fig.**
288 **4f**). Because previous studies have shown that perturbation both TFIIF and Rpb9 functions
289 results in upstream shifts (FURTER-GRAVES *et al.* 1991; HULL *et al.* 1995; SUN AND HAMPSEY
290 1995; SUN *et al.* 1996; KHAPERSKYY *et al.* 2008; EICHNER *et al.* 2010), the upstream-sensitive
291 reporter suppressor Rpb2 C317R could be consistent with disruption of this interface. Here,
292 Rpb2 C317 is buried, and substitution of an arginine might be predicted to perturb structure and
293 alter positioning of either Rpb9 or TFIIF or both. Disruption of Tfg1 at this interface
294 encompassing residue R422 (homologous to R417 in the studied *S. mikate* Tfg1)(EICHNER *et al.*
295 2010) and deletion of *RPB9* (WOYCHIK *et al.* 1991) each result in a cold sensitive phenotype, a
296 phenotype shared by Rpb2 C317R (**Fig. 3b**). In contrast to Rpb2 C317R, a nearby substitution
297 E319D results in the opposite phenotype – suppression of a downstream-shift sensitive
298 reporter. While Rpb2 E319 is close to Tfg1, it appears to make direct interactions with Rpb9 Y15
299 and R30 and perturbing the length of the 319 sidechain in E319D may alter this interaction with
300 Rpb9 (**Fig. 4e**).
301 We also isolated Rpb2 G369C and G369R mutants as upstream shifters (**Fig. 4f**).
302 Substitutions in Rpb2 G369 were previously isolated as Spt^- (HEKMATPANAH AND YOUNG 1991),
303 as a suppressor of a TFIIB downstream-shifting allele (CHEN AND HAMPSEY 2004), and to be
304 MPA^S with altered termination at a genetic reporter allele involving *ADH2* (KUBICEK *et al.* 2013).
305 Bulky substitutions for glycine at this residue would be in position to interfere with the Rpb1-Tfg1
306 interface (CHEN *et al.* 2007; SCHILBACH *et al.* 2021). Previous studies show that mutation in the
307 TFIIF dimerization domains within both Tfg1 and Tfg2 subunits also resulted in upstream TSS
308 shifts (SUN AND HAMPSEY 1995; GHAZY *et al.* 2004; EICHNER *et al.* 2010). Intriguingly, we also
309 isolated a downstream shifting mutation in the Pol II subunit Rpb10, a subunit shared amongst

310 three polymerases and that is discussed below where we probe how this substitution may be
311 working (**Fig. 6**).

312 Among GTFs, we identified novel alleles of *TFG2* (TFIIF), *SUA7* (TFIIB)*, RAD3, SSL1,*
313 *SSL2, TFB2*, *TFB4* and *TFB3* (TFIIH) and *TFA1* (TFIIE). For Tfg2, we identified three
314 suppressors of a downstream-shift sensitive reporter: V128G, C222Y (**Figs. 2b**, **4g**) and T366P
315 (**Supplementary Table 1**) (with C222Y isolated twice). This is the first occurrence of *tfg2* alleles
316 potentially conferring downstream shifts, because all previously identified mutants of TFIIF
317 resulted in upstream shifts (SUN AND HAMPSEY 1995; GHAZY *et al.* 2004; EICHNER *et al.* 2010).
318 Tfg2 V128 and C222 are close to each other in space but there is not an obvious interpretation
319 for their structural perturbations. Interestingly, while Tfg2 substitutions V128G and C222Y lie
320 within the Tfg2 dimerization domain (but not at the dimerization interface), T366P lies in the
321 winged helix domain (WH) and is not visualized in the yeast PIC. The WH domain has been
322 proposed to interact with upstream DNA (EICHNER *et al.* 2010).

323 In *SUA7,* we isolated novel suppressors of downstream-shift sensitive reporters in the B-
324 finger/B-reader domain such as R60W and G80R alleles as well as those in previously studied
325 residues R64K (BANGUR *et al.* 1997; PARDEE *et al.* 1998) and R78C (PINTO *et al.* 1994) (**Fig. 4h,**
326 **Supplementary Table 1**). We note that G80R is cold sensitive just as the classical *sua7* alleles
327 (PINTO *et al.* 1992b). Besides substitutions in the B-reader domain, we also identified R182C in
328 the Sua7/TFIIB B-core N-terminal cyclin fold (**Fig. S2**), the domain that interacts with the Pol II
329 wall, involved in directing the DNA-RNA hybrid (CRAMER *et al.* 2001; KOSTREWA *et al.* 2009).
330 The TFIIB B-core domain binds to the Pol II complex at the Rpb2 “wall” domain, which
331 undergoes reorganization as a consequence of the TFIIB-Pol II interaction. Previously isolated
332 substitutions in C149 at the TFIIB/Rpb2 interface resulted in a downstream TSS shift (WU *et al.*
333 1999). Our new substitution, Sua7 R182C is in a residue that packs with Sua7 C149, which is
334 adjacent to Rpb2 wall domain residue M868 (KOSTREWA *et al.* 2009; SAINSBURY *et al.* 2013)

335 (**Fig. 4h**). We also isolated Rpb2 substitutions in the wall near the N-terminal B-cyclin fold
336 domain proximal to M868 (Rpb2 G867S, Y931C, L961S). Unbiased isolation of TSS mutants at
337 this interface highlights the ability of our selections to identify interfaces involved in TSS
338 selection.

339 Within TFIIH, we isolated alleles across the complex, consistent with a network of
340 interactions throughout its subunits able to modulate the scanning process. Within Ssl1, *ssl1*
341 I122T and *ssl1* R230G were isolated and are the first *ssl1* alleles directly connected to TSS
342 selection. *SSL1* was initially genetically isolated through a suppressor of a stem loop placed at
343 the 5′ UTR of *HIS4* (YOON et al. 1992) and potentially regulates Rad3 helicase activity involved
344 in NER (COIN *et al.* 1998; KIM *et al.* 2015) via its VWA family protein domain. Rad3 activity is not
345 implicated in TFIIH initiation functions and the location of our *ssl1* alleles suggests that they
346 might instead alter internal Ssl1 interactions or the organization of residues that interact with
347 Tfb1 or Tfb4 or both. Ssl1 I122 is directly adjacent to a loop of Tfb4 that inserts into Ssl1 while
348 Ssl1 R230 is positioned internally to organize an Ssl1 loop that connects to both Tfb1 and Tfb4
349 interfaces (**Fig. 4i**).

350 Further, we isolated Tfb2 F189S that lies in the HEAT repeats domain of Tfb2, resulting
351 in suppression of a downstream shift-sensitive reporter. Tfb2 F189 contributes to hydrophobic
352 packing within Tfb2 that might limit dynamics or breathing of this critical connector protein for
353 bridging Ssl2 to the rest of TFIIH. Relaxation of this domain through loss of the bulky
354 phenylalanine sidechain potentially could confer flexibility on the connection of Ssl2 to the rest
355 of the complex (**Fig. 4k**). Similarly to how Tfb2 connects Ssl2 to the rest of TFIIH, Tfb4 is the
356 connector of Tfb2 to the rest of TFIIH. We isolated *tfb4* N71K as suppressor of a downstream
357 shift-sensitive reporter. Tfb4 N71 lies in the VWA domain and insertion of a bulkier and charged
358 lysine into an internal Tfb4 pocket might also loosen the Tfb4 structure, potentially adding
359 flexibility to the linkages across components (**Fig. 4k**).

360 Tfb3 is critical connecting TFIIH by its RING domain to Pol II (through Rpb7) and the rest
361 of the PIC (through TFIIE). Previously tested mutations that disrupt this interface cause
362 upstream shifts in TSS selection (YANG *et al.* 2022; YANG *et al.* 2024), while removal of the Tfb3
363 RING domain or the TFIIK kinase module (part of TFIIH) result in usage of TSSs ~30 bp
364 downstream of the TATA box in vitro, similarly to non-scanning eukaryotes (MURAKAMI *et al.*
365 2015; YANG *et al.* 2022). We have interpreted these mutants as conferring a defect in scanning,
366 either a loss of scanning processivity or reduction in scanning rate. Here, we have isolated *tfb3*
367 S23F as suppressing a downstream shift-sensitive reporter (**Fig. 4I**). Tfb3 residue S23 lies
368 within the Tfb3 RING finger domain and is present in a loop adjacent to a hydrophobic interface
369 with TFIIE subunits Tfa1 and Tfa2, formed by Tfb3 L22, Tfa1 I183, Tfa1 V102, Tfa1 H103, and
370 Tfa2 L283 (**Fig. 4I**). Intriguingly, a potentially more disruptive substitution at the very same
371 residue, *tfb3* S23P, was isolated as an upstream shifter along with other disruptive substitutions
372 at the Tfb3-TFIIE interface (YANG *et al.* 2022; YANG *et al.* 2024)(Basnet et al, in preparation).
373 Because it has the opposite phenotype of Tfb3 S23P, we interpret Tfb3 S23F as stabilizing the
374 Tfb3-TFIIE interaction (see Discussion). Supporting our interpretations of mutations identified in
375 targeted *TFB3* and *TFA1* genetic screens or site-directed mutational studies (YANG *et al.* 2022;
376 YANG *et al.* 2024)(Basnet et al, in preparation), we isolated mutations R64T and P51L in *TFB*3
377 that result in suppression of upstream shift-sensitive reporters, namely Tfb3 R64T and P51L
378 (**Fig. 3, 4I**). Tfb3 R64 had previously been identified as making a key interaction with Rpb7 and
379 each side of this interaction appears to function in promoting scanning as mutations are MPA^S
380 and/or alter TSS selection (BRABERG *et al.* 2013; YANG *et al.* 2022). Contemporaneously with
381 our identification of these residues in unbiased genetic selections, P51 mutations were directly
382 tested based on evolutionary analysis of *TFB3*, with P51 and R64 conferring strong MPA-
383 sensitivity. Because P51 and R64 substitutions were epistatic with each other, this result was
384 consistent with these residues working together, *e.g.* P51 working by enabling positioning of
385 R64 (YANG *et al.* 2024)**.**

386 For TFIIH, physical interactions between Rad3 and Ssl2 may also contribute to TFIIH
387 function in scanning (**Fig. 4j**). Rad3 K499E resulted in suppression of a downstream-shift
388 sensitive reporter and is directly proximal to Ssl2 (**Figs. 2b**, **4j**). We had previously identified
389 mutations in Ssl2 at K357R and K357E (ZHAO *et al.* 2021) near this Rad3 interface sharing the
390 same phenotype as Rad3 K499E, raising the possibility that could be functional interface, with
391 the caveat that Ssl2 K357 may act through other interactions. Because we interpret downstream
392 shifts for Ssl2 mutants as a gain of processivity, there are two possibilities for Rad3 K499E in
393 this framework. First, the interaction between Rad3 and Ssl2 might limit Ssl2 processivity, and
394 therefore we would interpret K499E as a loss of function for the interaction. Alternatively, the
395 interaction between Rad3 and Ssl2 might promote processivity, and K499E confers phenotypes
396 by strengthening the interaction.
397 We further wanted to isolate special "*ssl2*-like" alleles that showed both a His^+
398 phenotype on the downstream shift-sensitive *imd2Δ::HIS3* reporter and a Lys^+ phenotype due to
399 suppression of the *lys2-128∂* Spt^- phenotype reporter, a phenotype combination exhibited by a
400 specific subset of downstream-shifting *ssl2* mutants (ZHAO *et al.* 2021). These previously
401 identified alleles were highly localized to the DRD domain of Ssl2 (ZHAO *et al.* 2021). Before our
402 Ssl2 work, the Spt^- phenotype had only been observed in conjunction with upstream-shifting
403 phenotypes for alleles of Pol II and the TFIIF subunit Tfg2 (KAPLAN *et al.* 2012; JIN AND KAPLAN
404 2014). Because the Spt^- *ssl2* mutants appeared novel, we wanted to ask if additional GTF
405 mutants with similar phenotypes could be identified, therefore we performed selections with the
406 *imd2Δ::HIS3* reporter selecting on SC-His-Lys medium. While we identified two new alleles of
407 *SSL2*, each with a mutation in Helicase domain 1 (HD1, *ssl2* R378L and *ssl2* W482G), we did
408 not identify additional mutations of this class in other GTFs, suggesting this class of allele may
409 be unique to *SSL2*. Finally, we isolated a TFIIE mutation *tfa1* E374* as a putative downstream
410 shifting allele (**Fig. S2**). Tfa1 has been shown to have inhibitory effect on Tfa2-activated Ssl2
411 translocase activity (LIN AND GRALLA 2005). This suggests *tfa1* E374* could function by relieving

412 restriction on Ssl2 translocase activity, resulting in downstream TSS shift due to increased
413 processivity.
414
415 **Non-PIC mutants conferring suppression of TSS-shift sensitive reporters**
416 Besides PIC factors, our study also isolated non-PIC mutants, comprising putative reporter-
417 specific factors like guanine pathway mutants, indirect effectors like *PMR1*, and
418 chromatin/transcription elongation factors. We found almost fifty percent of initial *IMD2* reporter
419 suppressors had mutations in guanine metabolism genes (**Fig. 5a**). *IMD2* is activated under low
420 GTP conditions, specifically because low GTP induces a TSS switch that bypasses the
421 upstream terminator in the *IMD2* promoter (**Fig. 1a**). Therefore, defects in guanine metabolism
422 create inducing conditions for *IMD2.* We predicted this class of mutant might be differentially
423 sensitive to supplementation by guanine. We found that guanine supplementation suppressed
424 the His^+ phenotype of guanine pathway mutants specifically, but not a subset of tested PIC
425 mutants (**Fig. 5a**), and therefore incorporated guanine supplementation into subsequent
426 phenotyping conditions as indicated above. Our WGS also identified an allele of *PMR1* as a
427 suppressor of the *adhΔ50::HIS3* reporter (**Supplementary Table 1**). *PMR1* encodes an
428 ER/golgi Ca^{2+}/Mn^{2+} transporter, and loss of its activity raises cytoplasmic Mn^{2+} levels, conferring
429 Mn^{2+} hypersensitivity (RUDOLPH *et al.* 1989; DURR *et al.* 1998; MANDAL *et al.* 2000) (**Fig. 5b**).
430 Our lab had previously found that *pmr1*Δ genetically interacts with increased activity Pol II
431 mutants (BRABERG *et al.* 2013), that increased activity Pol II mutants are specifically sensitive to
432 increased Mn^{2+} (CABART *et al.* 2014), and that *pmr1*Δ itself resulted in an upstream shift to TSS
433 usage at the *ADH1* promoter (QIU *et al.* 2016), due to potential increased Pol II activity in
434 response to heightened cytoplasmic (and nuclear) Mn^{2+} levels. Isolating *pmr1* alleles as
435 suppressors of the *hmo1Δ38::HIS3* reporter would be consistent with potential global effects of
436 Mn^{2+} levels on TSS selection. While Mn^{2+} has many effects on Pol II transcription including
437 perturbing fidelity, it consistently stimulates RNA polymerase catalysis in vitro *e.g.* (NIYOGI *et al.*

438 1981; QIU *et al.* 2024). Therefore, upstream shifts at multiple promoters in vivo are consistent
439 with expectations for increased Pol II catalytic activity during initiation caused by increase in
440 cellular Mn^{2+} levels.

441 Intriguingly, we isolated chromatin-related Pol II associated elongation factors as
442 suppressors of both downstream reporters *imd2Δ::HIS3* and *cyc1-1019::HIS3* (**Fig. S3**). Many
443 of these are canonical "Spt" genes and fittingly, some of these were isolated in our double
444 selections for His^+ Lys^+ (Spt^-) suppressors, but a number were isolated from His^+ selections. We
445 isolated alleles of *spt2*, *spt5*, *spt16*, *bur2, spn1* and histones from both downstream-sensitive
446 reporters and *spt4* and *spt6* only from the *imd2Δ::HIS3* reporter (**Fig. S3**). This reporter bias
447 may potentially exist because our selections were not saturating. A role for Spt6 in *IMD2* TSS
448 selection has been described for specific *spt6* alleles defective for interaction with a
449 phosphorylated linker in Rpo21/Rpb1 (CONNELL *et al.* 2022). The chromatin/elongation factors
450 we isolated are all known to suppress initiation from cryptic promoters within genes (WINSTON *et*
451 *al.* 1984; CLARK-ADAMS *et al.* 1988; KAPLAN *et al.* 2003; CHEUNG *et al.* 2008; DORIS *et al.* 2018).
452 Similarly, their Spt^- phenotypes at *lys2-128∂* are consistent with a chromatinized-promoter within
453 a transcription unit (in this case, a Ty1 *∂* element within the *LYS2* gene) being activated upon
454 elongation-mediated chromatin disruption in specific mutants (SIMCHEN *et al.* 1984; WINSTON *et*
455 *al.* 1984; CLARK-ADAMS *et al.* 1988; SWANSON *et al.* 1991; PRELICH AND WINSTON 1993;
456 FISCHBECK *et al.* 2002; KAPLAN *et al.* 2003; CHEUNG *et al.* 2008; CUI *et al.* 2016; DORIS *et al.*
457 2018). This would be a reasonable model to explain suppression of *imd2Δ::HIS3* because the
458 *IMD2* promoter (driving His^+) is transcribed as part of an upstream CUT transcript (KOPCEWICZ
459 *et al.* 2007; JENKS *et al.* 2008; KUEHNER AND BROW 2008), potentially sensitizing the
460 downstream TSS to chromatin defects driven by Pol II elongation. Conversely, this model does
461 not easily explain why we also identified chromatin/elongation gene alleles as suppressors of
462 *cyc1-1019::HIS3* (see Discussion) and raises the possibility that chromatin factors might globally
463 alter TSS selection, which we test directly below.

464

465 **Functional characterization of TSS mutants through genetic interaction analyses**

466 After our genetic selections, we wanted to functionally characterize mutants using genetic
467 interactions. In our prior studies, both additive/synergistic and epistatic interactions have been
468 observed for TSS-shifting mutants leading to a framework where mutants are interpreted as
469 affecting initiation efficiency (i.e. Pol II catalysis) or scanning processivity (TFIIH/PIC functions).
470 Previous examination of double mutants between Pol II catalytic mutants and TFIIB or TFIIF
471 alleles showed additivity across combinations (enhancement when mutants shift TSSs the same
472 direction and suppression when they shift in opposite directions). However, in other
473 combinations, we observed epistasis where double mutants exhibited the TSS phenotype of
474 one of the single mutants and not the other. This was especially clear when upstream shifting
475 Pol II mutants were combined with downstream shifting *ssl2* alleles, leading to the hypothesis
476 that the tested *ssl2* alleles increase scanning processivity, but this didn't lead to downstream
477 TSS shifts in mutants that increase initiation upstream. Regardless of mechanistic models for
478 how mutants are genetically interacting, double mutant analysis can reveal when mutations are
479 dependent on one another (epistasis), which is indicative of their defects being at the same
480 step, or when mutations function redundantly in an essential step (synergy or synthetic lethality),
481 or when mutations are perturbing a system independently, whereby double mutant phenotypes
482 will be the additive consequences of the single mutants combined. To therefore functionally
483 dissect our mutants, we tested interactions at inter-subunit interfaces and further analyzed
484 functional interactions across the PIC (**Figs. 6b, 6c; 7; S4**).

485 We first tested a potential Rpb10-Tfg1 interface in TSS selection by genetic interaction
486 studies and site-directed mutagenesis. We isolated *rpb10* L25S as a downstream-shifting
487 suppressor of the *imd2Δ::HIS3* reporter and showed this allele could also suppress the *cyc1-*
488 *1019::HIS3* reporter (**Fig. 2b**). Because Rpb10 is a common subunit shared amongst three RNA
489 polymerases, it was interesting to find a Pol II-specific phenotype. Examination of Pol PIC

490 structures for Pol I, II, and III PICs suggested that an interaction between Rpb10 in the vicinity of
491 the Rpb10 helix-loop-helix L25 residue might only be present in the Pol II PIC, where Rpb10
492 appears to contact a loop in the Tfg1 N-terminal domain (**Fig. 6b**). This potential interaction
493 suggested that Rpb10 might affect Pol II TSS distributions through an interaction with TFIIF
494 subunit Tfg1 that may be perturbed in the *rpb10* L25S allele. To examine this, we targeted
495 Rpb10 E29 and Tfg2 R26 residues that display potential interactions based on structural studies
496 (SCHILBACH *et al.* 2021) (**Fig. 6c**). We generated a series of genomic mutations by CRISPR
497 including charge reversals at both of these residues and assessed growth and TSS-shift
498 reporter phenotypes. On analysis of mutants, we did not observe overall growth defects in *tfg*1
499 single or *tfg1 rpb10* double mutants (**Fig. 6c**, rows 6 and 7). Charge reversal *rpb10* mutation of
500 E29R resulted in suppression of the downstream shift reporter while E29A did not display
501 effects (**Fig. 6c**, rows 3 and 4). However, when *rpb10* E29R was combined with the *tfg1* R26A
502 or R26E mutations, apparent suppression of the downstream shift phenotype was observed
503 (**Fig. 6c**, rows 10 and 11). Moreover, we found that *tfg1* mutants also suppressed the leaky His^+
504 phenotype of *imd2Δ::HIS3*, with Tfg1 R26E being more robust than R26A (**Fig. 6c**, rows 6 and
505 7, SC-His panel). Suppression of the leaky His^+ phenotype of *imd2Δ::HIS3* might result from an
506 upstream TSS-shifting phenotype, therefore we tested these *tfg1* mutants against the upstream
507 reporter *adhΔ50::HIS3* (**Fig. 6c**, lower panel) but *tfg1* mutants did not suppress *adhΔ50::HIS3*.
508 These results show that an additional *rpb10* allele can alter TSS selection (**Fig. 6c**) and that its
509 phenotype can be modulated by proximal *tfg1* alleles. However, we could not prove that Rpb10-
510 Tfg1 interactions underlie the *rpb10* L25S mutant phenotype.

511 We tested additional functional interactions by tetrad dissection analysis of diploids
512 followed by fitness analysis of each spore by pixel quantification. We then calculated "expected"
513 double mutant growth phenotype from single mutant phenotypes by a multiplicative model for
514 independent effects on fitness of single mutants in a double mutant combination (MANI *et al.*
515 2008) and compared this expected double mutant growth phenotype to the observed double

516 mutant growth phenotype. Genetic interactions were established based on comparisons of
517 these double mutant metrics. We examined upstream shifting *rpb9*Δ genetic interactions with a
518 panel of mutants. First, we examined *rpb9*Δ in conjunction with the upstream-shifting *rpb2*
519 G369C as the proximity of Rpb9 to Rpb2 and TFIIF raises the possibility that these mutants
520 work in the same pathway, as it has previously been proposed that *rpb2 G369C* works through
521 effects on TFIIF. Second, we tested *rpb9*Δ against a subset of our novel downstream shifting
522 alleles to ask if they were additive or epistatic. The GTF TFIIF binds at the interface between
523 Rpb9 and Rpb2 in the protrusion-lobe domain with proximity to Rpb2 G369 (**Fig. 4, 7b**)(CHEN *et*
524 *al.* 2007). Because *rpb2* G369C and *rpb9*Δ are both upstream shifting mutations, it is expected
525 that the double mutant in case of non-interaction would be a product of individual fitnesses.
526 Conversely, if they functioned together in the same process, we might observe less than
527 multiplicative effects (sometimes referred to as a specific form of epistasis). Instead, we
528 observed growth fitness of *rpb2* G369C *rpb9Δ* double mutants to be worse than predicted from
529 the multiplicative model, indicating a synthetic defect (**Fig. 7d**).
530 When combining upstream shifting *rpb9*Δ with a panel of downstream shifting mutants,
531 we confirmed a subset of those with *tfg2* C222Y, *rad3* K499E and *tfb2* F189S by tetrad
532 dissection analysis (**Fig. S4**). We found *rpb9Δ tfg2* C222Y double mutant fitness to be slightly
533 worse than expected (**Fig. S4**, left panel). Because these mutants have opposite effects on TSS
534 shifts, combination might be predicted to result in suppression of growth defects, if the effects of
535 each mutant on TSS selection are additive *and* the growth defects observed correspond to the
536 TSS selection phenotype. Conversely, if either of the *tfg2* C222Y or *rpb9*Δ effects require a WT
537 allele for their specific phenotypes, then instead of suppression of phenotypes by two opposite
538 acting alleles, we might observe exacerbation due to conversion of a downstream or upstream
539 shifting allele to the other in the double mutant. Assuming the change in growth fitness reflects
540 an equivalent change in TSS selection, this kind of interaction could represent sign epistasis.

541 In contrast to the *rpb9*Δ-*tfg2* C222Y negative interaction, we observed clear double mutant
542 suppression between *rpb9Δ rad3* K499E and *rpb9Δ tfb2* F189S where each TFIIH allele
543 suppressed growth defects associated with *rpb9*Δ (**Fig. S4**, middle and right panels). This
544 indicates that the growth defect induced by upstream mutant *rpb9Δ* was compensated by both
545 downstream mutants *rad3* K499E and *tfb2* F189S, while also suggesting that the growth defect
546 of *rpb9*Δ could be initiation-related because of its suppression by two alleles of TFIIH. This
547 result was unexpected based on a simple model where the *rpb9*Δ upstream-shifting phenotype
548 may be caused by loss of its restraint of the key Pol II catalytic domain, the trigger loop. This
549 model was based on *rpb9*Δ conferring similar phenotypes to hyperactive mutants in the Rpb1
550 TL (upstream TSS shifts and increased elongation rate in vitro). Upstream-shifting trigger loop
551 mutants are epistatic to downstream-shifting *ssl2* TFIIH alleles so similar interactions between
552 *rpb9*Δ and downstream-shift reporter specific-TFIIH alleles was what was previously expected
553 (see Discussion).
554
555 **Novel PIC alleles shift TSSs genome wide while chromatin/elongation alleles have muted**
556 **effects**
557 To gain insight into the function of a subset of our TSS shifting mutants, we quantified TSSs
558 across a curated set of promoters genome wide by STRIPE-seq in WT and mutant strains
559 (POLICASTRO *et al.* 2020; POLICASTRO *et al.* 2021; POLICASTRO AND ZENTNER 2022) (**Fig. 8a**).
560 We chose 8 downstream-shifting mutants, six from the PIC class and two from the
561 chromatin/elongation class isolated in our studies namely *tfb4* N71K, *rad3* K499E, *ssl1* I122T,
562 *tfb2* F189S, *rpb1* A480S, and *rpb1*0 L25S (PIC mutants) and *spn1* V199G and *spt5* G814*
563 (chromatin/elongation mutants) together with their corresponding WT parents (**Figs. 8**, **9**, **S5**,
564 **S6**). To assess TSS shifts in mutants relative to WT parents, we quantified TSSs as in our
565 previous studies (QIU *et al.* 2020; ZHAO *et al.* 2021) along with STRIPE-seq processing as in
566 (POLICASTRO *et al.* 2021). We focused our TSS analyses to 5979 Pol II promoter regions (RHEE

567 AND PUGH 2012; QIU *et al.* 2020; ZHAO *et al.* 2021) filtered to include promoters passing a cutoff
568 of a read count threshold in the promoter window analyzed resulting in analysis of n=2829
569 promoters. TSS usage values were then compared to those in WT by two TSS shift metrics as
570 in (QIU *et al.* 2020; ZHAO *et al.* 2021): shift in median TSS (Δ median), which represents the
571 difference in median position of the TSS distribution at a promoter between a mutant and WT
572 strains (**Fig. 8b**) and change in spread (Δ spread) that represents the change in width of
573 promoter TSS distributions relative to WT (**Fig. 9a**).

574 Individual replicates were generally reproducible for Δmedian TSS (**Fig. S5**). Principal
575 component analysis (PCA) of the Δmedian values of combined replicates showed three clusters
576 representing functional differences across the primary axis of variance (**Fig. 8c**): cluster 1
577 contained *rpb1* A480S, *rpb10* L25S, *ssl1* I122T and *tfb4* N71K, cluster 2 contained *rad3* K499E
578 and *tfb2* F189S, and cluster 3 contained *spt5* G814* and *spn1* V199G. When examining PCA of
579 individual replicates each compared to the average WT median position (**Fig. S5b**)**,** we found
580 chromatin alleles to cluster near the WT, suggesting they only have mild effects on TSS
581 distributions globally, but with greater effects for *spt5* G814* than for *spn1* V199G (**Fig. 8f**).
582 While both chromatin/elongation alleles had effects more broadly than just the individual
583 reporter, their effects were quantitatively and qualitatively different from PIC alleles, consistent
584 with potentially relating to the chromatin context of individual promoters rather than innately
585 affecting TSS selection and promoter scanning at all promoters. All PIC alleles showed a large
586 bias towards downstream shifts in TSS distribution across the majority of promoters, with *rad3*
587 K499E and *tfb2* F189S showing the strongest effects (**Fig. 8f**).

588 PCA of Δspread values also displayed three groups and examination of PCA for
589 individual replicates of all strains compared to the average WT behavior shows that
590 chromatin/elongation mutants cluster with WT, most PIC mutants cluster together while *rad3*
591 K499E and *tfb2* F189S, which showed the strongest effects on Δmedian TSS, formed a
592 separate cluster based on Δspread (**Figs. 9, S6**). Examination of directional bias in spread

593 suggests that while spread was perturbed for most mutants, *rad3* K499E and *tfb2* F189S
594 showed the strongest increase in spread, consistent with the downstream shift in TSS usage
595 also expanding TSS spread to downstream positions (**Figs. 9e, S6d**). These results again
596 differentiated two TFIIH alleles, *rad3* K499E and *tfb2* F189S, from two others, *ssl1* I122T and
597 *tfb4* N71K.
598

599 **DISCUSSION**

600 Our studies reveal the wider landscape of genes and specific mutations that can alter the TSS
601 selection landscape in yeast. In addition to independently identifying some already discovered
602 alleles, validating our novel reporters, we also identified a wide array of novel alleles
603 suppressing our initiation reporters. Notably, we did not find additional factors associated with
604 promoters but not directly connected to the PIC, such as chromatin remodelers or transcription
605 coactivators, as able to suppress our initiation reporters. We find that mutations in many PIC
606 components including Rpb10 and additional TFIIH subunits that can perturb initiation by
607 promoter scanning when mutated. Importantly, we find that the novel *rpb10* allele and tested
608 TFIIH alleles alter TSS selection genome wide. Our prior studies, new alleles identified here,
609 and in our parallel studies on the Pol II/PIC interface reinforce that upstream shifting of TSSs
610 results from compromise of TFIIH-PIC interactions through the Tfb3-TFIIE-Rpb7 interface
611 (BRABERG *et al.* 2013; YANG *et al.* 2022; YANG *et al.* 2024) Basnet et al, in preparation). We
612 extend evidence that the Rpb2-TFIIB interaction is important for promoter scanning while also
613 finding that perturbation to Rpo21/Rpb1 and Rpb2 broadly leads to suppression of downstream-
614 shift sensitive reporters. This latter result further supports the idea that defective Pol II
615 catalysis/initiation activity results in phenotypes consistent with downstream shifts in TSS
616 usage. In contrast, we also have identified novel TFIIH downstream-shifting alleles that are
617 generally not located at inter-subunit interfaces, save one.

618 The downstream-shifting phenotype of these novel TFIIH alleles would be consistent
619 with a gain of function in TFIIH scanning processivity or rate. One interpretation of our alleles in
620 Rad3, Tfb2, Tfb4, and Ssl1 based on their locations is that they alter plasticity or dynamics
621 within the TFIIH structure. When this plasticity is altered, perturbations may propagate either to
622 the Ssl2 active site or to Ssl2 DNA binding properties, which in turn allow scanning to be
623 extended to downstream positions through increased processivity or increased scanning rate.
624 The idea that TFIIH processivity can be sensitive to small structural perturbations provides a
625 conceivable evolutionary path for TFIIH to gain ability to reach downstream TSSs during the
626 advent of the promoter scanning mechanism.
627 Potential communication between Ssl2 and the rest of the PIC can take a few paths.
628 First, there is a connection from Ssl2 to Tfb3 and Pol II/TFIIE through the following proteins:
629 Ssl2 to Tfb2 to Tfb4 to Ssl1 to Rad3 to Tfb3. Second, Tfb1 drapes over multiple TFIIH
630 components and connects to Tfa1 from TFIIE. Finally, Rad3 has a small number of residues
631 that may close the gap between it and Ssl2 and contact Ssl2 residues. We have identified
632 alleles along components that form the path from Ssl2 to Tfb3 (Tfb2, Tfb4, Ssl1, Tfb3) and
633 between Rad3 and Ssl2. If the protein connection between Ssl2 to Tfb3 has a certain amount of
634 flexibility or dynamics (using an analogy of an accordion's bellows or a pantograph that might
635 tolerate or allow extension or contraction, depending on rigidity), then alterations to this flexibility
636 might have consequences for Ssl2 rate or processivity as it translocates downstream on
637 promoter DNA. The locations of putative gain of function Tfb2, Tfb4, and Ssl1 alleles are all
638 consistent with perturbing internal intra-subunit interactions and we would propose they
639 increase flexibility of the "bellows" or "pantograph" formed by these components that connect
640 Ssl2 to Tfb3 and the PIC. This increased flexibility may then allow Ssl2 to translocate longer or
641 faster, resulting in a shift in TSS usage to downstream positions. Future biochemical and
642 biophysical experiments, potentially coupled with molecular dynamics simulations, might provide

643 tests of a model that, first, novel TFIIH alleles do indeed confer increased TFIIH processivity,
644 and second, that these alleles might alter structural properties of TFIIH in similar ways.
645 Chromatin/elongation factors can be envisioned to function in controlling initiation in two ways.
646 First, native chromatin architecture may reduce transcription initiation from nucleosome-
647 occluded TSSs (most yeast promoters have TSSs located within the boundaries of +1
648 nucleosomes) (RANDO AND WINSTON 2012). If there are downstream shifts in nucleosomes
649 dependent on elongation factors, then this could feed back to TSS usage and relax nucleosomal
650 inhibition of nucleosome-sensitive TSSs for promoters with appropriately positioned +1
651 nucleosomes. Second, if a promoter's TSSs are transcribed themselves from an upstream
652 promoter, then promoter-associated nucleosomes that are transcribed dependent on an
653 upstream TSSs could become dependent on factors that restore transcribed nucleosomes in the
654 wake of elongating Pol II. This situation might reflect allele-selective effects on TSS usage for
655 transcribed promoters and less so global effects. This arrangement of an upstream promoter
656 driving transcription of a downstream promoter and thereby sensitizing the chromatin over the
657 downstream promoter is similar to that observed at the *SRG1-SER3* locus (MARTENS *et al.*
658 2004) and also the structure of the *lys2-128∂* allele (SIMCHEN *et al.* 1984). Each of these loci are
659 especially sensitive to chromatin and transcription elongation defects, and the latter of which
660 was used in the original identification of a number of the Spt chromatin/elongation factors –
661 factors that we isolated with our reporters here (SIMCHEN *et al.* 1984; CLARK-ADAMS AND
662 WINSTON 1987; CLARK-ADAMS *et al.* 1988; MALONE *et al.* 1991; SWANSON *et al.* 1991; CUI *et al.*
663 2016). In these cases, chromatin maintenance suppresses transcription initiation from within the
664 transcribed regions. Altered chromatin architecture in chromatin mutants can result in
665 widespread initiation from cryptic promoters (PRELICH AND WINSTON 1993; KAPLAN *et al.* 2003;
666 CHU *et al.* 2007; CHEUNG *et al.* 2008; DORIS *et al.* 2018) but perhaps also from chromatin-
667 sensitive TSSs adjacent to existing promoters. In either case, altered chromatin can result in
668 increased transcription from "suppressed" sites.

669 We rationalize the identification of chromatin elongation factors from the *imd2Δ::HIS3*
670 reporter because of its idiosyncratic transcription from upstream TSSs (generating a cryptic
671 unstable transcript (CUT)(DAVIS AND ARES 2006; KOPCEWICZ *et al.* 2007; JENKS *et al.* 2008;
672 KUEHNER AND BROW 2008)) that likely contributes to or controls nucleosome positioning over the
673 downstream, low-guanine inducible TSS. It was already known that certain *spt6* alleles could
674 increase usage of downstream TSSs at *IMD2* in the absence of known inducing conditions
675 (CONNELL *et al.* 2022). Here, we extend identification of chromatin and elongation factors that
676 can act at *IMD2* through suppression of *imd2Δ::HIS3* to *spt2*, *spt4*, *spt5*, *spt16*, *spn1*, *bur2, hta1,*
677 and *htb1* alleles. These results suggest that *imd2Δ::HIS3* may be similarly sensitive to the
678 chromatin/Spt$^-$ class of mutant as is the classical *lys2-128∂* allele. However, we also isolated
679 chromatin mutants suppressing *cyc1-1019::HIS3* in addition to *imd2Δ::HIS3.* This *cyc1* allele
680 was inserted into a non-native locus that is devoid of genes that has previously been used to
681 house reporter genes (GRUBER *et al.* 2012). Our initial presumption was that the *CYC1* promoter
682 would not be itself transcribed, but examination of data from the Steinmetz lab (XU *et al.* 2009)
683 suggests that our *CYC1* promoter fragment also contains *SUT215*, a stable unannotated
684 transcript, and that integration of *cyc1-1019::HIS3* at chrI:199270-199271 causes it to be
685 flanked by *SUT004* upstream and *CUT442* downstream. Taken together, these provide support
686 that *cyc1-1019::HIS3* sensitivity to chromatin and elongation factors could be through
687 transcription over its promoter altering promoter nucleosomes.
688
689 **Limitations of the study**
690 Our genetic interaction analysis indicated some interesting relationships between reporter
691 suppressor alleles, specifically the suppression observed between a subset of downstream-
692 shifting TFIIH alleles and *rpb9Δ*. Our previous genetic interaction studies showed that upstream
693 shifting Pol II catalytic alleles were epistatic to downstream-shifting *ssl2* alleles for both growth
694 phenotypes and for TSS shifts at *ADH1* (ZHAO *et al.* 2021). Our previous understanding for

695 *rpb9*Δ was that it was functioning similarly to upstream-shifting Pol II catalytic alleles (KASTER *et*
696 *al.* 2016). This assumption, coupled with the assumption that novel downstream-shifting TFIIH
697 alleles should function like *ssl2* downstream-shifting alleles, led to the expectation that *rpb9*Δ
698 would be epistatic to TFIIH alleles for TSS shift phenotypes. Additionally, we had the
699 expectation that *rpb9*Δ growth phenotypes related to its elongation defects and would not
700 necessarily be suppressible by initiation factor mutants. Contrary to these expectations, we find
701 the possibility of complexity in genetic interactions that might indicate different initiation alleles
702 are working in more complex ways than we had previously thought. Because the TFIIH alleles
703 that showed suppression also showed greater magnitude of TSS shifts than those that did not,
704 we do not know if suppression by some TFIIH alleles but not others relates to allele-specific
705 differences in function or simply allele strength. We imagine these results should be developed
706 and extended in a few ways. First, more comprehensive double mutant analyses of the novel
707 TFIIH alleles and *rpb9*Δ would allow differentiation of the two alleles where we observe strong
708 suppression of *rpb9*Δ from others to determine allele specificity. Second, double mutant
709 combinations of *rpb9*Δ and existing *ssl2* alleles and of Pol II alleles with novel TFIIH alleles
710 would also allow understanding of potential allele specificity. Third, examination of double
711 mutants for phenotypes on transcription reporters to assess if initiation specific phenotypes
712 reflect overall growth phenotypes. Finally, quantitative primer extension analysis of double
713 mutants for *ADH1* TSS selection would also determine if growth phenotypes correlate with
714 specific changes to TSS distributions at promoters.
715

716 **MATERIALS AND METHODS**

717 **Yeast strains and oligos**

718 Yeast strains and oligos used in this study are listed in **Supplementary Table 2**.

719 **Yeast media**

720 Yeast media used in the current studies have been prepared as previously described in

721 (AMBERG *et al.* 2005; KAPLAN *et al.* 2012; JIN AND KAPLAN 2014; MALIK *et al.* 2017; ZHAO *et al.*
722 2021). Briefly, all solid media contain 2% w/v agar (BD); YPD is 1% w/v yeast extract (Gibco™
723 Bacto™), 2% w/v peptone (Gibco™ Bacto™) and 2% w/v glucose (VWR) supplemented with
724 0.15 mM adenine (Sigma) and 0.4 mM tryptophan (Sigma) for solid medium (not supplemented
725 when liquid); YPD+3% formamide contains 3% v/v formamide (Ambion); YP Raffinose (YPRaf)
726 and YP Raffinose Galactose (YPRafGal) contain 2% w/v raffinose (Amresco) (YPRaf) or 1% w/v
727 galactose (Sigma) and 2% w/v raffinose (YPRafGal). Both YPRaf and YPRafGal are additionally
728 supplemented with 1 µg/ml of (Sigma) Antimycin A to prevent aerobic respiration. Synthetic
729 minimal media (SC-) were what is referred to as "Hopkins mix" with minor alterations as
730 previously noted (AMBERG *et al.* 2005; KAPLAN *et al.* 2012) (amino acid dropout mix, 0.17% w/v
731 yeast nitrogen base w/o amino acids and 0.5% w/v ammonium sulphate (BD), 2% glucose), with
732 the appropriate dropouts. Mycophenolic acid (MPA) (Thermo scientific chemicals) containing SC
733 media were supplemented at 20 µg/ml. Other drugs in the respective media were: G418
734 (GoldBio) and clonNAT (GoldBio) at 200 µg/ml, hygromycin (GoldBio) at 300 µg/ml and
735 canavanine at (Sigma) 60 µg/ml. Synthetic minimal media containing G418, clonNAT or
736 hygromycin are prepared as above with 0.1% w/v of monosodium glutamate (MSG) replacing
737 ammonium sulphate. Drug 3-aminotriazole (3AT) (Sigma) a competitive inhibitor of His3p was
738 used in some SC-His media at varying concentrations (later noted), for setting threshold for
739 visible His^+ phenotype.

740 **Genetic selections**

741 Each of the genetic selection strains possessing initiation reporters was grown overnight in
742 liquid YPD. Cultures were then washed twice in sterile distilled water to remove residual amino
743 acids before plating on respective selection media. Selection media for the reporters were SC-
744 His + 2mM 3AT for *imd2Δ::HIS3* and SC-His + 0.1mM 3AT for *cyc1-1019::HIS3*, *adhΔ50::HIS3*
745 and *hmo1Δ38::HIS3*. For selection of His^+Lys^+ candidates for downstream reporters, conditions
746 used were SC-His-Lys +5mM 3AT for *imd2Δ::HIS3* SC-His-Lys +0.1mM 3AT, Cells were spread

747 using sterile 3mm glass beads at 10^8 cells per plate. Multiple colonies of each parent strain were
748 inoculated for genetic selection to increase changes of independent candidates. Plates were
749 then kept in a lightly sealed plastic bag to prevent drying out and incubated at 30˚C for ~7 days
750 until suppressor colonies appeared.

751 **Single spot phenotyping**

752 Suppressor candidates were picked from selection plates and spotted onto solid YPD petri plate
753 in 8x6 grid (48-well format) containing 2 parents and 46 candidates apiece for the purpose of
754 candidate rescreening and additional phenotyping. Briefly, after growth on YPD, cells were
755 transferred into 100 µl of sterile distilled water in a 96-well tray using a 48-pin replicator,
756 followed by a second dilution of 6 µl of this cell suspension into 150µl of water. A sterilized 48-
757 pin replicator was then used to spot from the 150µl cell suspension onto phenotyping media.
758 Phenotype scoring timing was day 2 for YPD 30˚C and YPD 37˚C, day 3 for YPD+3%
759 formamide and synthetic complete medium (SC), day 4 for YPRaf, day 5 for SC-Lys and YPD at
760 16˚C and day 6 for YPRafGal. Reporter phenotypes on SC-His +/- 3AT were scored on days 3
761 through 5 depending on strength and SC-His-Lys +/- 3AT on day 5. **Scoring:** Scoring was
762 performed as in Jin & Kaplan 2014. Single phenotype spots were given scores from 0 to 5,
763 where 0 means no growth and 5 is WT parent growth on complete medium. For conditional
764 phenotypes where growth is indicative of mutant phenotype (i.e. Spt^- phenotype or His^+
765 phenotypes in reporter strains), scoring was 0 for no growth (WT) with positive numbers
766 indicating increasing growth reflecting strength of mutant phenotype. Relative scores of mutants
767 were first calculated per condition by $Score_{mutant}$-$Score_{WT}$ (Relative $score_{mutant:\ condition}$). These
768 relative scores were then corrected to respective control growth condition for estimating mutant
769 score corrected to control condition (e.g.: Relative $score_{mutant:\ YPRafGal}$ - Relative $score_{mutant:\ YPRaf}$).
770 These would assign positive values to mutants where growth is better than WT, negative to
771 those where growth is worse in an any condition and a 0 to WT.

772 **Mutation validation by re-introduction:**

773 Mutations were reintroduced into a clean parental strain possessing relevant initiation reporter
774 to validate effects of candidate mutations on reporter expression. Mutations were amplified from
775 suppressor strains and fused with a drug resistance marker by PCR sewing to generate a
776 *mutation::drug resistance marker* cassette and reintroduced into parent strains (JANKE *et al.*
777 2004). Marker used was KanMX6 containing insulated resistance cassettes (pFA6a-KanMX6-
778 ins2) to minimize potential effects of marker expression on adjacent loci (POWERS *et al.* 2022).
779 Multiple independent transformants were phenotyped and genotyped to assess correlation of
780 reporter suppression and introduction of the mutant genotype along with the resistance marker.
781 The marker was also used to tag mutation loci to enable synthetic genetic array analysis and
782 selection of mutant loci through genetic crosses. CRISPR based mutagenesis was performed to
783 generate *rpb10* and *tfg1* mutations in the genome as described in (LAUGHERY *et al.* 2015).

784 **Diploid generation**

785 Complementation assays and genetic interaction studies were performed with diploid
786 generation. Diploids were generated by mating suppressor candidates against parent or mutant
787 strains of opposite mating type, followed by double selection of individual haploid markers for
788 selecting diploids. Briefly, candidate suppressors, pre-integrated with auxotrophic markers
789 (*LEU2* for *MATalpha* and *TRP1* for *MATa*) were mated with the opposite mating type of the
790 required strains with a second auxotrophic selection marker; or appropriate drug resistance
791 markers were used for diploid selection for genetic interactions. Mating was performed by
792 transferring solid YPD-grown candidates to pre-aliquoted 100 µl-per-well of saturated culture of
793 test strain per well in a 96-well plate using a 48-pin (8x6) replicator and spotting onto solid YPD
794 using the same replicator. Post incubation for 2 days at 30˚C on plates, cells were transferred
795 into 100µl of pre-aliquoted sterile distilled water with the 48-pin replicator and resuspended by
796 shaking of replicator followed by transfer onto a double-selection media. These were incubated
797 at 30˚C to select for diploids for 2 days.

798 **Double mutant generation by synthetic genetic array**

799 Double mutants were generated from diploids of "tagged" single mutants mated in high
800 throughput following protocol from the Boone lab
801 (https://boonelab.ccbr.utoronto.ca/pdf/SGA_protocol_final.pdf). Briefly, a panel of *MATα single*
802 *mutation 1::drug resistance marker 1* strains was mated to a query *mutation 2::drug resistance*
803 *marker 2 MATa* strain possessing a *MATa* marker *can1Δ::STE2pr-URA3,* and diploids were
804 selected by double drug resistance as aforementioned. After two days of incubation on double
805 drug diploids were transferred from solid medium directly onto solid enriched sporulation media
806 (1% potassium acetate enriched with auxotrophic amino acids in 2% agar) for 5 days at 27˚C.
807 After sporulation, sporulated spots were transferred into 50 µl sterile distilled in 96 well plate
808 using a pinner, resuspended and spotted onto haploid selection media (SC-Ura-
809 Arg+MSG+canavanine), single mutant selection media (SC-Ura-Arg+MSG+canavanine + drug
810 1 or drug 2) and double mutant (SC-Ura-Arg+MSG+canavanine+drug 1+drug 2) selection media
811 in parallel instead of the traditional approach where mutants (single or double) are selected after
812 *MATa* meiotic progeny selection in tandem. We have observed that sicker haploids are lost if
813 selections are performed in tandem.

814 **Genomic DNA sequencing**

815 Candidate mutations were identified via AmpliSeq-based custom amplicon sequencing and
816 whole genome sequencing (WANG *et al.* 2025). Genomic DNA was isolated from candidates
817 using PureLink™ Pro 96 Genomic DNA Purification Kit and YeaStar genomic DNA kit from
818 Zymo research for AmpliSeq based sequencing. Plasmid miniprep kit from Zymo research,
819 customized with bead lysis was used for genomic DNA isolation for whole genome sequencing.
820 AmpliSeq libraries were prepared and sequenced by the Texas A&M TIGGS genomics core
821 facility. AmpliSeq libraries were prepared following AmpliSeq for Illumina protocol for a custom
822 oligo pool comprising 1917 encompassing 310 genes. These genes comprise ORFs of
823 transcription machinery and transcription-associated genes. Libraries were sequenced in

824 batches of 96 samples using full Illumina MiSeq of 15 million reads by 250bpx2 run to aim for an
825 average coverage of ~80X per amplicon. Whole genome sequencing of samples was performed
826 by Seqcoast or Seqcenter. Each genomic DNA sample was sequenced at a depth of 400Mbp
827 yielding an average coverage of ~30X.

828 **AmpliSeq data processing**

829 Paired-end sequencing fastq files were first trimmed for adaptors at the 3' end, followed by 3'
830 and 5' oligo trimming (amplification oligos do not contribute towards mutation detection) by
831 cutadapt v2.1 (MARTIN 2011). These were then processed by MutantHuntWGS v1.1 (ELLISON *et*
832 *al.* 2020), a container-based package deploying predefined tools for alignments and variant
833 calling. Briefly, oligo and adaptor-free paired-end fastq files were aligned to *Saccharomyces*
834 *cerevisiae* S288C reference genome R64-2-1 by bowtie2 v2.2.9 (LANGMEAD AND SALZBERG
835 2012) resulting in bam alignment files followed by bam sorting and indexing by SAMtools v1.3.1
836 (LI *et al.* 2009; DANECEK *et al.* 2021). Genotype likelihoods were calculated followed by variant
837 calling by BCFtools v1.3.1 (DANECEK *et al.* 2021) using haploid ploidy file provided by
838 MutantHuntWGS v1.1 (ELLISON *et al.* 2020). This resulted in vcf files for all sequenced
839 candidates. Mutant variants in mutant vcf files were differentially called relative to parent vcf files
840 by VCFtools v 0.1.14 (DANECEK *et al.* 2011). Resulting differential mutants were annotated
841 using SNPeff v4.3p (CINGOLANI *et al.* 2012) and SIFT4G (VASER *et al.* 2016), which uses
842 EF4.74 *Saccharomyces cerevisiae* library for annotating severity of amino acid change. For
843 WGS, fastq reads were analyzed by Seqcenter and Seqcoast for mutation detection by breseq
844 (DEATHERAGE AND BARRICK 2014). *Saccharomyces cerevisiae* S288C reference genome R64-1-
845 1 was used for annotation which generated a list of variants. Variants specific to suppressor
846 candidate were curated by a custom shell script comparing mutant variants to parent variants.

847 **STRIPE-seq**

848 Total RNA was isolated from 50ml of mid-log yeast culture with density of $1X10^7$ cells/ml as
849 described previously (SCHMITT *et al.* 1990) and resuspended in 90µl nuclease free water. RNA

850 samples were in-column DNase I treated using RNeasy mini kit from Qiagen with 100µg input
851 per column. DNased RNA (10µg per sample) were depleted of rRNA using bioltinylated
852 riboPOOL kit for *Saccharomyces cerevisiae* from siTOOLS Biotech, purified by Dynabeads
853 MyOne Strptavidin C1 and eluted in 9µl nuclease free water. STRIPE-seq libraries were then
854 generated from rRNA depleted RNAs using 200ng RNA per sample as previously published
855 (POLICASTRO *et al.* 2020) with our modifications. Briefly, 200ng of each RNA sample, split into
856 two 100ng reactions were terminator exonuclease (TEX) treated to remove uncapped RNA.
857 Pooled TEXed reaction was then reverse transcribed using a random 10-mer with partial
858 homology to P7 adaptor RTO (GCCTTGGCACCCGAGAATTCCANNNNNNNNNN) instead of a
859 complete P7:oligo-random pentamer (modification; P7 adaptor added during final library
860 amplification). Non-templated cytosines at the 3' end of cDNA then allow annealing of a
861 template switching oligo, containing partial P5 adaptor, 9-base UMI (instead of 8-base UMI) and
862 a linker (TATAGGG) (Biotin-
863 GTTCAGAGTTCTACAGTCCGACGATCNNNNNNNNNTATArGrGrG). After template switching,
864 libraries were amplified by dual indexing primers with complete P5 and P7 adpators. Libraries
865 (>200-800bp) were extracted from 3% polyacrylamide TBE gel to remove oligos and then
866 sequenced by Illumina NextSeq 2000 system with 1X50bp sequencing cycle. Sequencing reads
867 were delivered demultiplexed.

868 **STRIPE-seq analysis**

869 STRIPE-seq fastq files were processed as TSS-seq reads we had previously published (ZHAO
870 *et al.* 2021) with STAR alignment and additional bam processing followed previously published
871 of goSTRIPES and TSRexploreR packages (POLICASTRO *et al.* 2020; POLICASTRO *et al.* 2021;
872 POLICASTRO AND ZENTNER 2022). Fastq files were filtered for quality with fastx-toolkit v 0.0.14 (-
873 q 20 -p 75) (http://hannonlab.cshl.edu/fastx_toolkit/), followed by trimming of adaptors by
874 trimmomatic v 0.38 (BOLGER *et al.* 2014) and then 9 base UMI extraction by umi-tools v 1.0.0
875 (SMITH *et al.* 2017). Reads were then trimmed of linker TATAGGG and then trimmed to 25

876 bases by cutadapt v 2.10 (MARTIN 2011) before local alignment by STAR v 2.7.9a (DOBIN *et al.*
877 2013) generating bam files. Bam files with uniquely mapping reads were then filtered of
878 unfavorably flagged reads by samtools v 1.9 (samtools view –F 3844) (LI *et al.* 2009; DANECEK
879 *et al.* 2021) followed by deduplication by umi-tools v 1.0.0 (SMITH *et al.* 2017). Deduplicated and
880 indexed bam files were then processed by the protocol followed by the Zentner lab (POLICASTRO
881 *et al.* 2020; POLICASTRO *et al.* 2021; POLICASTRO AND ZENTNER 2022). Briefly, reads with more
882 than 3 soft-clipped 5' bases are listed and filtered out by picard v 2.18.12 (Picard Toolkit 2019)
883 following GoSTRIPES (Robert Policastro). Indexed filtered bams were then processed by
884 TSRexploreR (POLICASTRO *et al.* 2021) for G correction to generate bedgraphs for 5' ends of
885 reads (TSSs) that we processed to split into + and – strand bedgraphs and downstream
886 analyses following our TSS-seq pipeline (ZHAO *et al.* 2021). Pearson correlation matrices were
887 generated for bedgraphs of all libraries using our in-house Rscript. Promoter matrices
888 representing TSSs were generated comprising 401 base window (250 bases upstream and 150
889 bases downstream from median TSS position including the median) across 5979 annotated
890 promoters (RHEE AND PUGH 2012). These matrices were utilized for estimating median and
891 spread (base distance between 10th and 90th percentile) of TSS distributions across the 5979
892 promoter and eventually Δmedian and Δspread of mutants relative to WT for differences (ZHAO
893 *et al.* 2021). Promoter matrices were row normalized before generating average matrices across
894 replicates and estimating average median and average spread values for calculating average
895 Δmedian and Δspread values relative to average WT. Top 2829 promoters with expression
896 cutoff of 10 were selected based on library normalized average of all WTs sorted by expression:
897 sum of TSSs per 401 base promoter window.

898 **Data availability**

899 Sequencing data generated in this study are available in the NCBI BioProject under accession
900 number PRJNA1337182.

Acknowledgements

We acknowledge funding from National Institutes of Health grants R01GM120450 and R35GM144116 to C.D.K. We acknowledge Dr. David Brow at the University of Wisconsin for guidance on genetic selections. We are especially grateful to the students of BIOSC 0068 Foundations of Biology Laboratory 2 course at the University of Pittsburgh for genetic selection of candidates leading to identification of a subset of alleles described here. We acknowledge Gabe Zentner, Robert Policastro, and Chhabi Govind for advice on STRIPE-seq. We would like to dedicate this paper to the memory of Gabe Zentner.

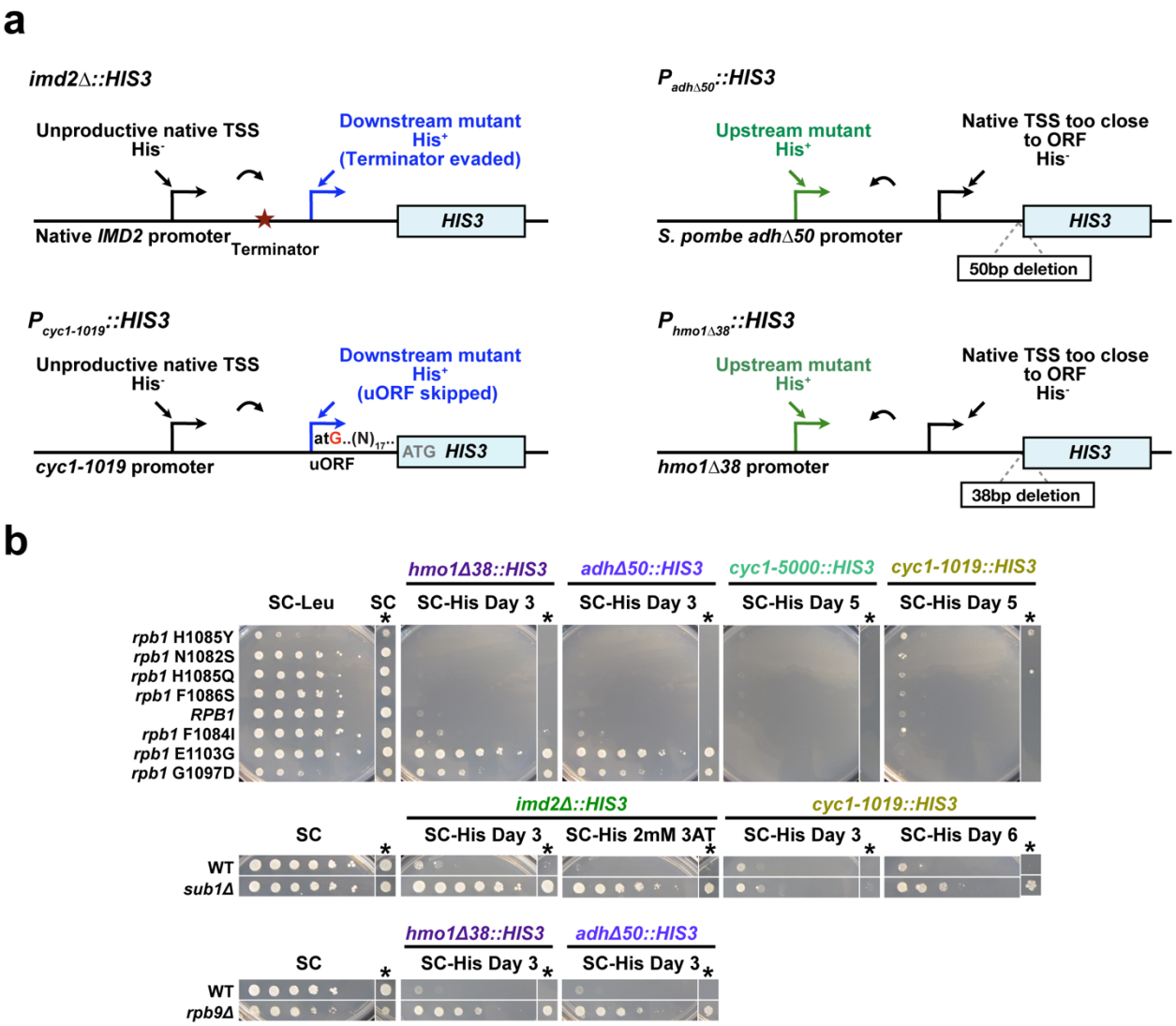

Figure 1. TSS shift-sensitive reporters detect TSS shifts by *HIS3* expression. a. Schematic of initiation reporters *imd2Δ::HIS3* and *cyc1-1019::HIS3* sensitive to downstream shifts in TSS usage. Downstream-shifting TSS mutants constitutively express *IMD2* transcripts from a downstream TSS that allows functional *HIS3* expression when *HIS3* replaces the *IMD2* ORF, conferring a His$^+$ phenotype (top). Downstream TSS shifts at *cyc1-1019::HIS3* allow an upstream AUG to be bypassed, resulting in usage of the appropriate in-frame AUG, allowing functional His3p translation (bottom). **Right.** Schematic of the initiation reporters *adhΔ50::HIS3* (top) and *hmo1Δ38::HIS3* (bottom) that are sensitive to upstream shifts in TSS usage. Truncation places the native TSSs for these promoters too close to the native AUG rendering ineffective translation initiation. Upstream shifts in TSS selection lengthen the 5′ UTRs for each reporter, allowing His3p to be translated from the lengthened *HIS3* mRNA. **b.** Validation of reporter phenotypes with known TSS-shifting mutants: 10-fold serially diluted yeast strains or a single concentration of cells (marked with asterisk – "single spot phenotyping") are plated on media to illustrate reporter function. *rpb1* alleles (upstream or downstream shifts), *sub1Δ* (downstream shift), and *rpb9Δ* (upstream shift) mutants were tested against the upstream and downstream shift sensitive reporters to illustrate allele-specific reporter activity.

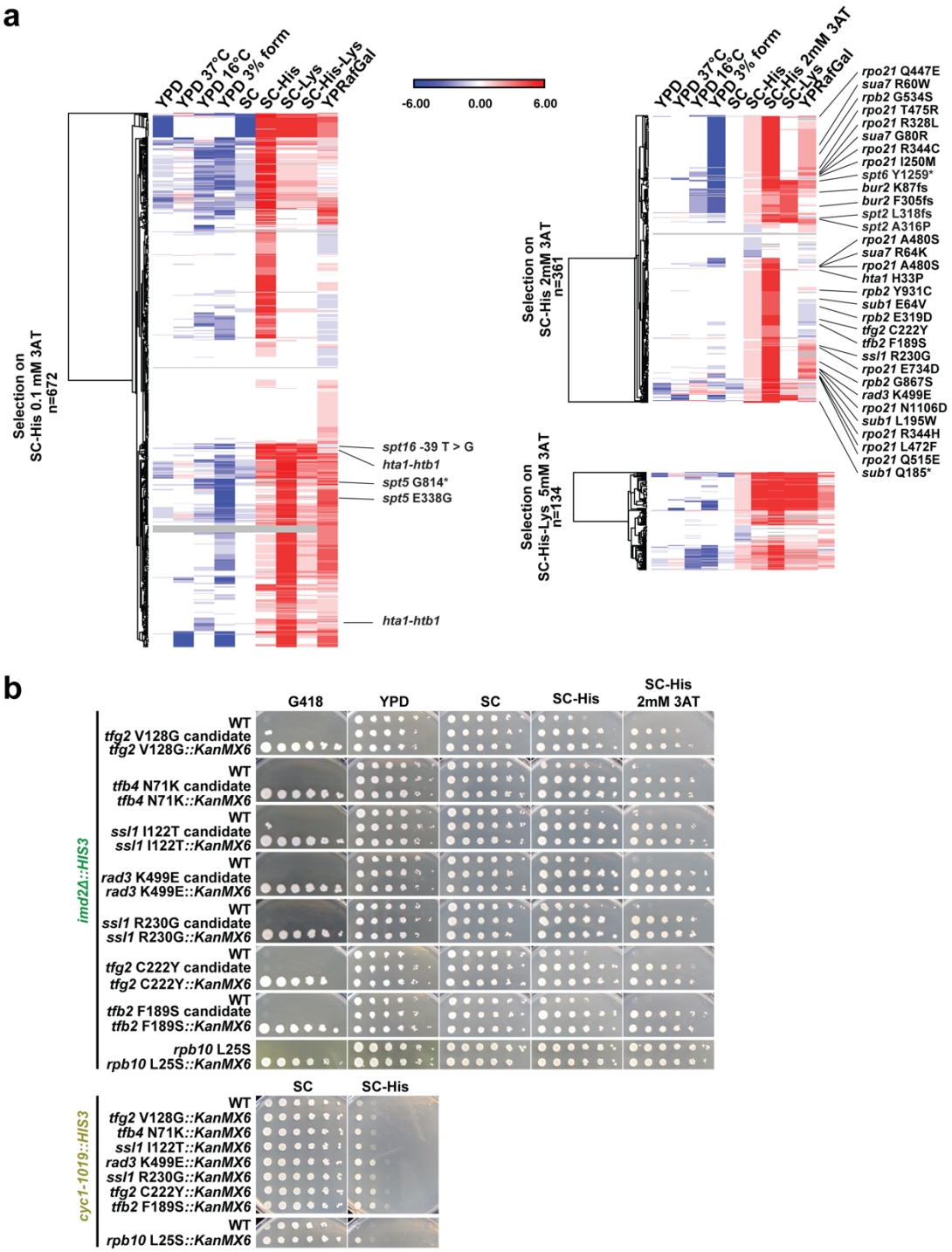

Figure 2. Isolation of spontaneous suppressors of downstream TSS-shift sensitive initiation reporters. a. Hierarchically clustered phenotypes of a subset of candidate downstream-shifting suppressors of *cyc1-1019::HIS3* (left) or *imd2Δ::HIS3* (right) reporters with a subset of identified mutations annotated; right bottom panel displays *imd2Δ::HIS3* suppressors isolated by selection on SC-His-Lys+5mM 3AT. **b.** Validation of a subset of candidates by knock-in of TSS mutants into *imd2Δ::HIS3* and *cyc1-1019::HIS3* reporter backgrounds and re-phenotyping. Mutations were amplified out of isolated candidates, PCR

934 sewed with a drug marker cassette and re-introduced into each of the reporter strains by
935 integrative transformation. The *rpb10* candidate mutation was introduced using CRISPR/Cas9.

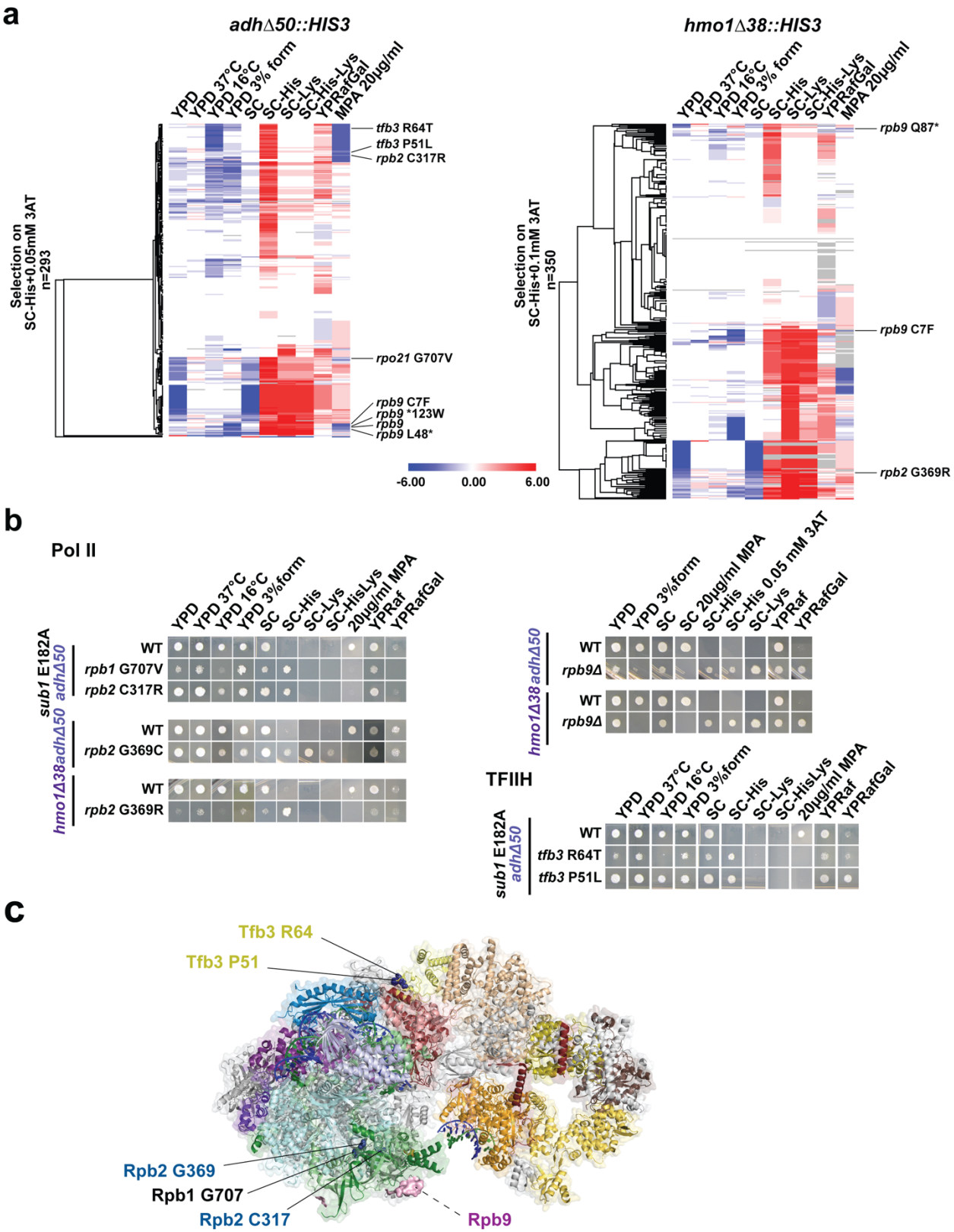

Figure 3. Isolation of spontaneous suppressors of upstream TSS-shift sensitive initiation reporters. a. Hierarchically clustered single-spot phenotypes of a subset of upstream-shifting

939 suppressors of *adhΔ50::HIS3* (left) and *hmo1Δ38::HIS3* (right) initiation reporters with identified
940 mutations annotated. **b.** Single spot phenotyping of upstream isolated mutants. **c.** Cryo-EM
941 structure of Pol II PIC annotated with upstream shifting mutation residues identified.

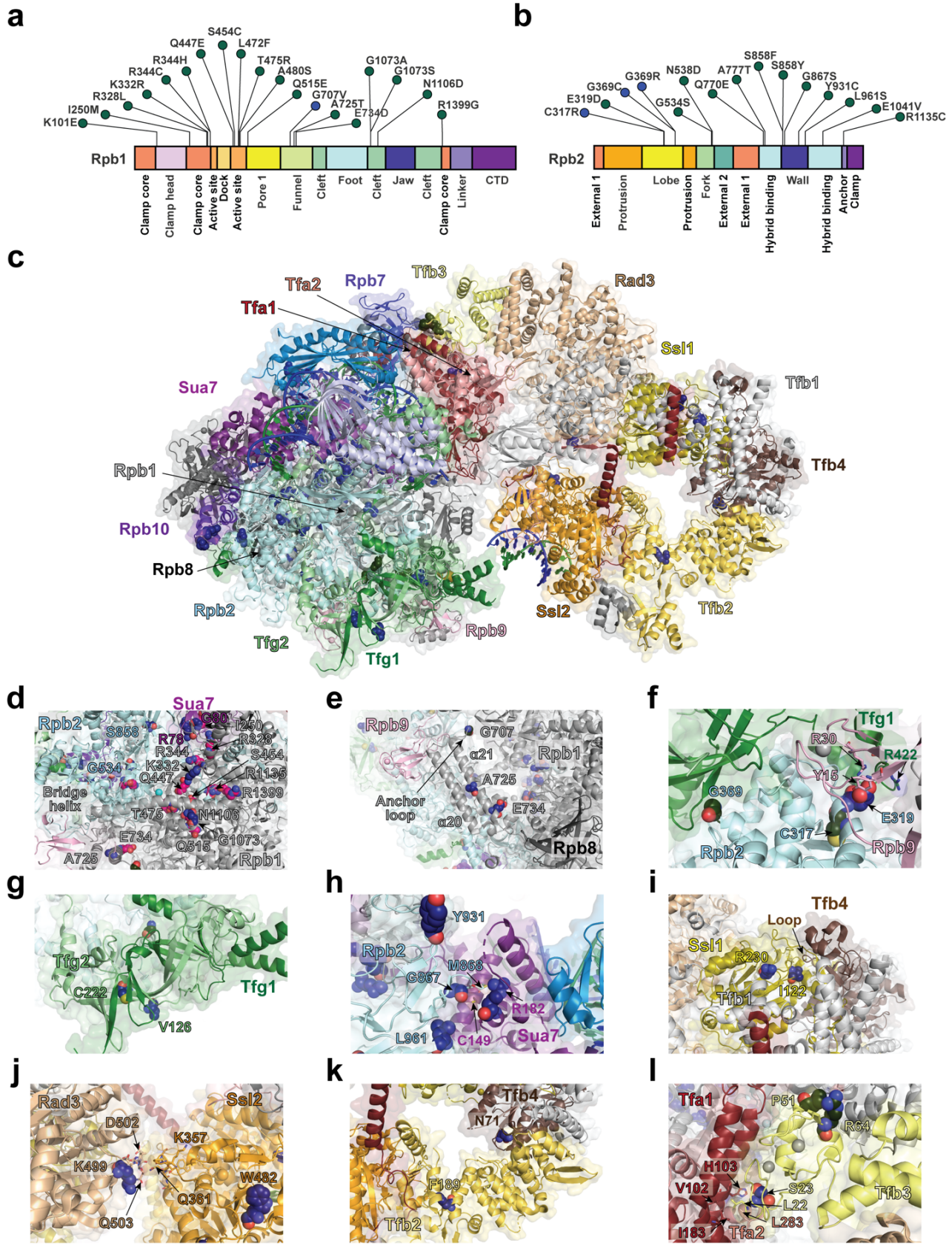
a
S454C
Q447E
L472F
R344H
T475R
R344C
A480S
G1073A
K332R
Q515E
G1073S
R328L
G707V
N1106D
I250M
A725T
R1399G
K101E
E734D
Rpb1
Clamp core
Clamp head
Clamp core
Active site
Dock
Active site
Pore 1
Funnel
Cleft
Foot
Cleft
Jaw
Cleft
Clamp core
Linker
CTD
b
S858F
A777T
S858Y
G867S
G369R
N538D
G369C
Q770E
Y931C
E319D
G534S
L961S
C317R
E1041V
R1135C
Rpb2
External 1
Protrusion
Lobe
Protrusion
Fork
External 2
External 1
Hybrid binding
Wall
Hybrid binding
Anchor
Clamp
c
Tfa2
Rpb7
Tfb3
Rad3
Tfa1
Ssl1
Sua7
Tfb1
Rpb1
Tfb4
Rpb10
Rpb8
Rpb2
Ssl2
Tfb2
Rpb9
Tfg2
Tfg1
d
Sua7
Rpb2
C80
I250
S858
R78
R828
R344
S454
G534
K332
R1135
Q447
R1399
Bridge helix
T475
N1106
E734
G1073
Q515
A725
Rpb1
e
Rpb9
G707
α21
Rpb1
A725
Anchor loop
E734
α20
Rpb8
f
Tfg1
R30
R422
Y15
G369
E319
C317
Rpb2
Rpb9
g
Tfg2
C222
Tfg1
V126
h
Y931
Rpb2
M868
G867
R182
L961
C149
Sua7
i
Tfb4
Loop
Ssl1
R230
I122
Tfb1
j
Rad3
Ssl2
D502
K357
K499
W482
Q361
Q503
k
Tfb4
N71
F189
Tfb2
l
Tfa1
P51
R64
H103
V102
S23
L22
Tfb3
L283
I183
Tfa2

942

943 **Figure 4. Mutations identified across PIC**. Lollipop diagram of mutations isolated in Rpb1 (**a**)
944 and Rpb2 (**b**). Domain diagram figure created using IBS 2.0 (XIE *et al.* 2022). **c**. PIC structure
945 (PDB: 7O4J) displaying mutations isolated in our study. **d.** Structural mutations surrounding
946 active cleft that are formamide sensitive marked in magenta. **e.** Mutations in α21 helix and
947 anchor loop isolated with proximity to Rpb9 and Rpb8. **f.** Residues at Rpb2-TFIIF-Rpb9
948 interface found to alter TSS selection. **g.** Initiation mutations near Tfg1-Tfg2 interface causing
949 downstream shifts. **h.** Mutations altering interactions between Sua7 B-core and Rpb2 isolated in
950 this study in the vicinity of previously isolated Sua7 C149 initiation mutant. **i.** Potential
951 interactions between Ssl1 and Tfb4 loop or Tfb1 in driving TSS selection. **j.** Rad3 K499E
952 mutation potentially driving TSS selection by altering interactions with Ssl2 across Rad3-Ssl2
953 interface with K357R and K357E previously isolated in our study altering TSS selection. **k.**
954 Mutations in Tfb2 F189 and Tfb4 N71 lying within the respective structural domains potentially
955 promoting structural "breathing". **l.** Mutation S23F in the RING domain of Tfb3 increasing
956 interaction between TFIIH and TFIIE by potentially promoting allele-specific hydrophobic
957 packing.

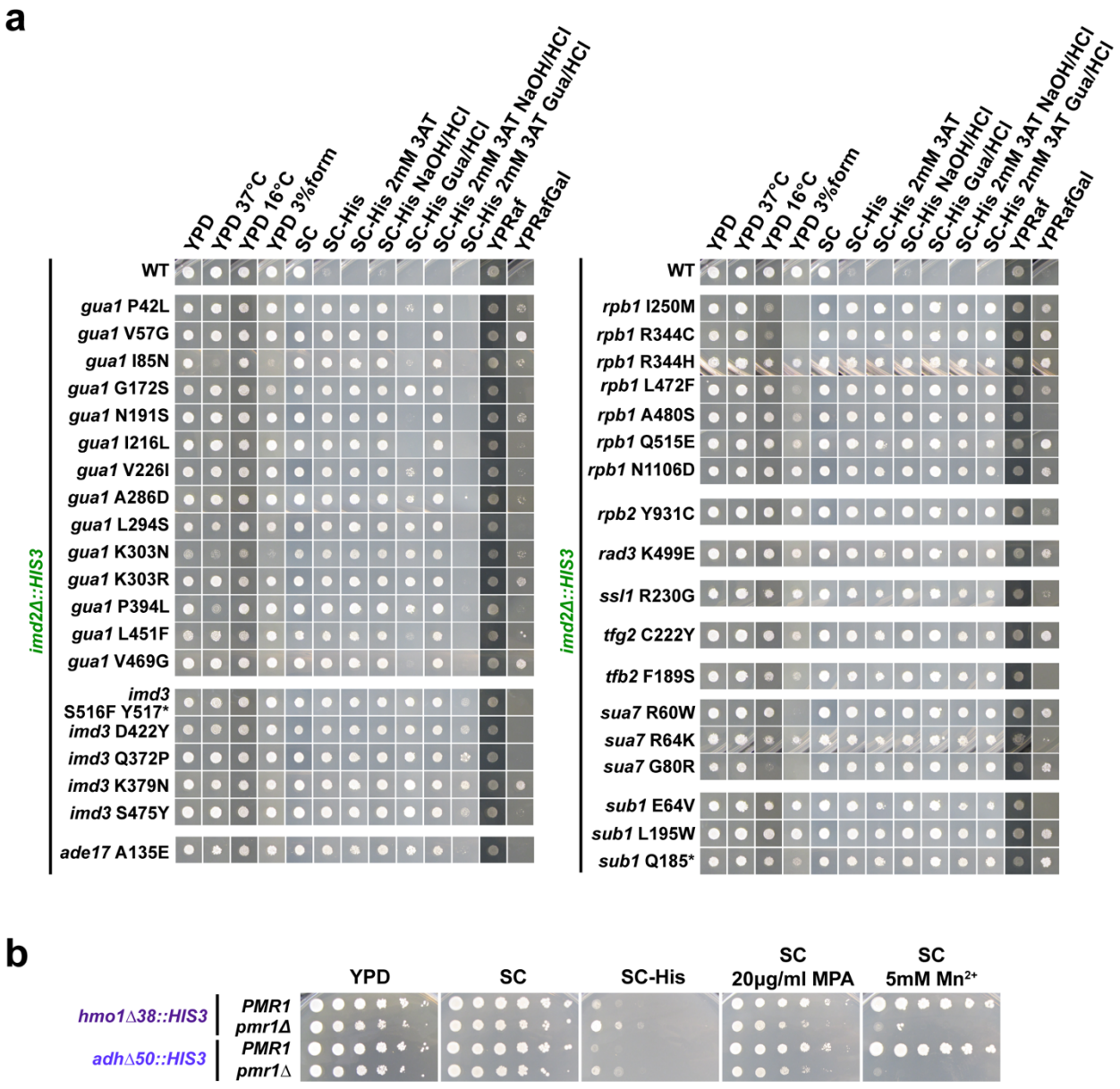

Figure 5. Phenotyping of subset of non-PIC mutants identified as suppressors of initiation reporters. a. Guanine metabolism mutants and controls plated as single concentrations of cells on phenotyping media. Guanine metabolism gene mutants confer the His$^+$ phenotype to cells with the *imd2Δ::HIS3* reporter, likely due to the *IMD2* promoter's sensitivity to guanine levels. Guanine supplementation suppresses the His+ phenotype of guanine pathway mutants (SC-His 2mM 3AT Gua/HCl: left panel) whereas PIC mutants remain His$^+$ under the same conditions (SC-His 2mM 3AT Gua/HCl: right panel). Guanine is solubilized in 10mM NaOH at a final concentration of 500µM and media must be neutralized by equivalent HCl as NaOH alone affects solubility of MPA. **b.** 10-fold serial dilutions of *PMR1* or *pmr1Δ* strains plated on phenotyping media. *pmr1Δ* suppresses both upstream reporters and confers sensitivity to Mn^{2+}.

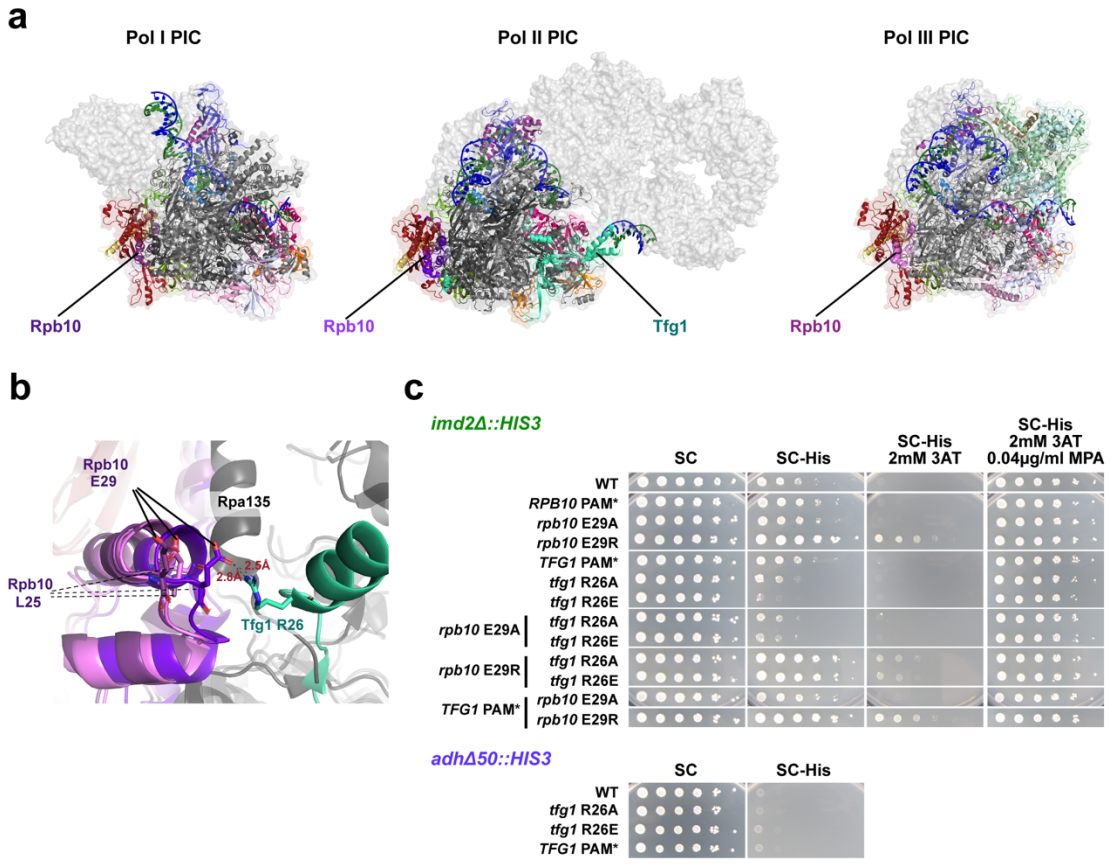

Figure 6. Analysis of potential Rpb10-Tfg1 interactions in proper TSS selection. a. Cryo-EM structures of PICs of Pol I, Pol II, and Pol II displaying Rpb10, a shared subunit between them. **b.** Cryo-EM structure of Rpb10 from Pol I-III PICs (Pol I PIC: 6TPS, Pol II PIC: 7O4J, Pol III PIC: 6EU0) overlayed displaying Tfg1 from the Pol II PIC, with Tfg1 R26 in the proximity of Rpb10 E29 suggesting a potential electrostatic interaction. While Rpa135 in Pol I lies adjacent to Rpb10, a specific physical interaction with Rpb10 E29 may not exist. **c.** Serially diluted spot assay phenotyping of single and double mutants of *tfg1* R26 and *rpb10* E29 resides displaying charge reversals and mutations to alanine and silent PAM control mutations as mutants were generated by CRISPR/Cas9.

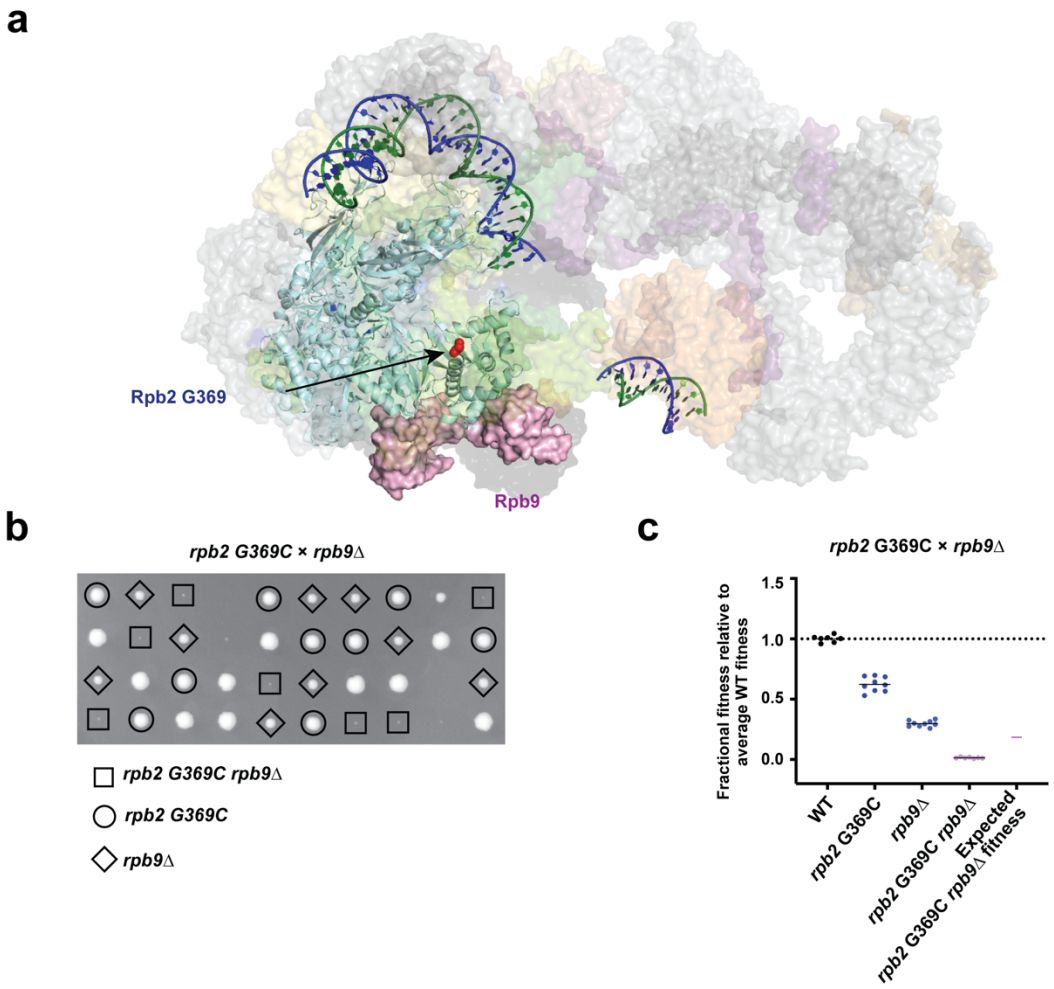

Figure 7. Synthetic genetic interaction between *rpb9Δ* and *rpb2* G369C. a. Cryo-EM structure of Pol II PIC displaying Rpb2 G369 and Rpb9. Rpb2 G369 lies in the Pol II lobe domain which interacts with Rpb9 though this region between Rpb2 and Rpb9 and has been shown to interact with TFIIF. **b.** Tetrad dissection of *rpb9Δ*/+ *rpb2* G369C/+ diploid to examine genetic interactions between them. Spores are annotated by genotype. **c.** Observed and expected fitness of single and double mutants plotted for assessing genetic interaction. "Expected" fitness for a double mutant is the product of the two single mutant fitnesses (MANI *et al.* 2008). Observed fitness of single and double mutants estimated by quantification of spore colony sizes. Observed fitness is worse than expected fitness indicating a synthetic genetic interaction.

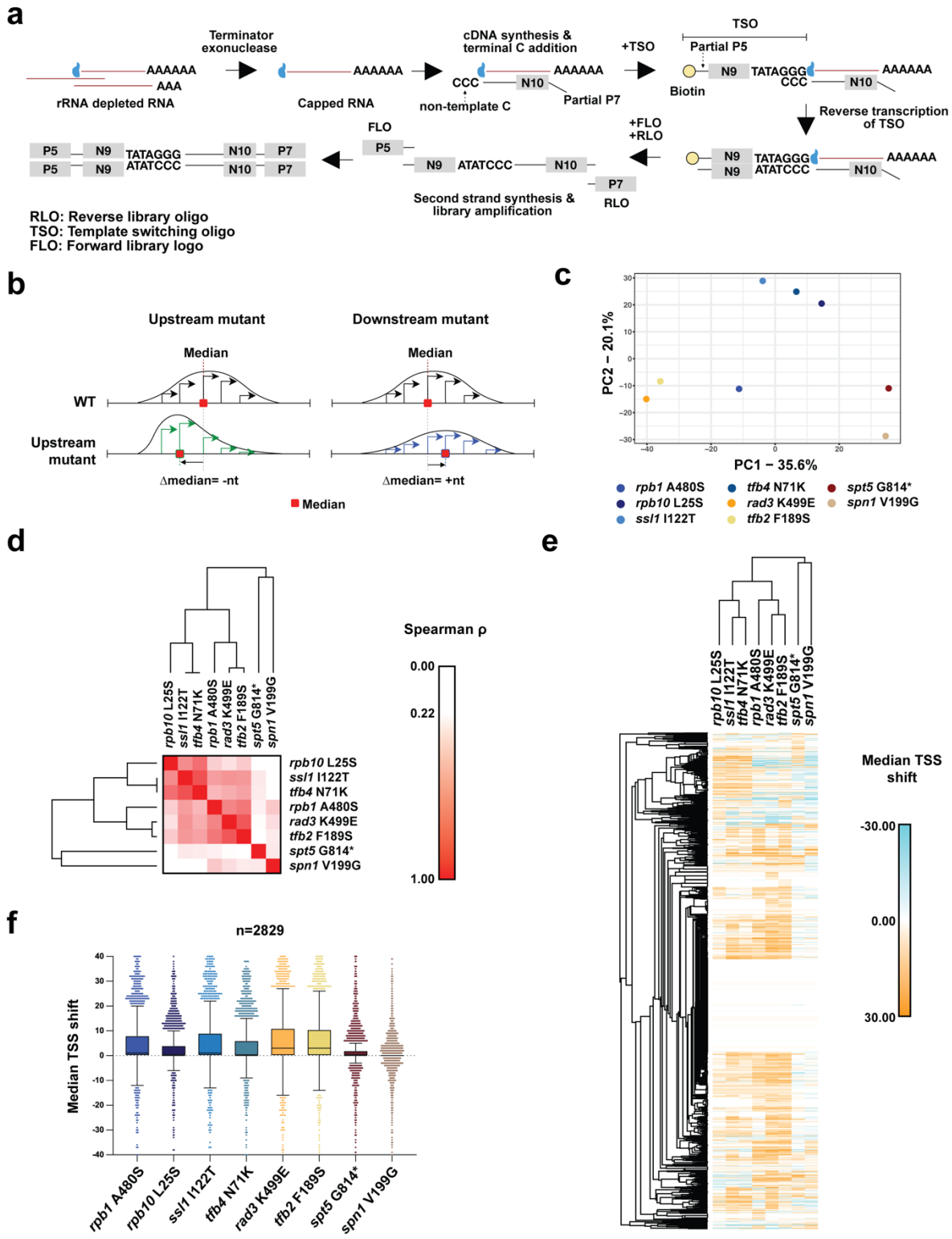
a
Terminator exonuclease
cDNA synthesis & terminal C addition
+TSO
TSO
Partial P5
AAAAAA
AAA
rRNA depleted RNA
Capped RNA
CCC
N10
non-template C
Partial P7
N9
TATAGGG
CCC
Biotin
Reverse transcription of TSO
+FLO
+RLO
FLO
P5
N9
ATATCCC
P7
RLO
Second strand synthesis & library amplification
RLO: Reverse library oligo
TSO: Template switching oligo
FLO: Forward library logo
b
Upstream mutant
Downstream mutant
Median
WT
Upstream mutant
Δmedian= -nt
Δmedian= +nt
c
PC2 – 20.1%
PC1 – 35.6%
rpb1 A480S
rpb10 L25S
ssl1 I122T
tfb4 N71K
rad3 K499E
tfb2 F189S
spt5 G814*
spn1 V199G
d
Spearman ρ
0.00
0.22
1.00
e
Median TSS shift
-30.00
0.00
30.00
f
n=2829
Median TSS shift

992

993 **Figure 8. STRIPE-seq analysis of novel mutants identifies three functional groups of**
994 **initiation mutants based on shift of median of TSS distribution. a.** Schematic of STRIPE-
995 seq library generation. **b.** Schematic of ∆median metric for TSS analysis. **c.** Principal
996 component analysis (PCA) of ∆median values of the top 2829 promoters based on an
997 expression cutoff of ≥10 reads within the analyzed 401 nucleotide promoter windows. PCA of
998 ∆median values across mutants with combined biological replicates plotted along the first two
999 principal components display three clusters, ① chromatin mutants *spt5* G814*, *spn1* V199G, ②
1000 *rpb1* A480S, *rpb10* L25S, *ssl1* I122T, *tfb4* N71K and ③ *rad3* K499E and *tfb2* F189S. **d.**
1001 Hierarchical clustering of Spearman correlation of ∆median values across mutants. **e.**
1002 Hierarchically clustered heatmap of ∆median values across top 2829 promoters of mutants with
1003 replicates combined. **f.** Box-plot analysis of ∆median values across mutants presented by Tukey
1004 plot.

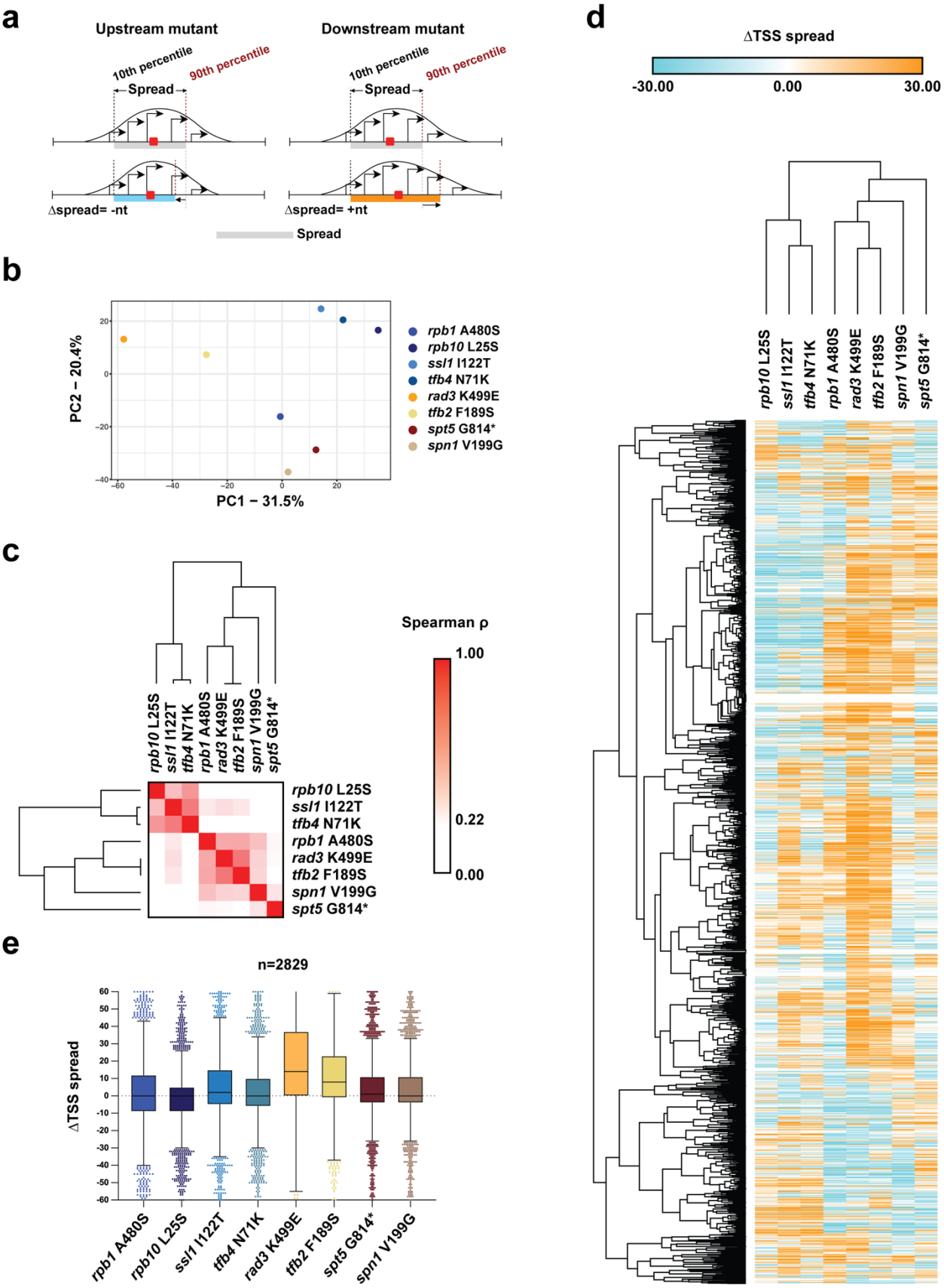
a
Upstream mutant
Downstream mutant
10th percentile
90th percentile
Spread
Δspread= -nt
Δspread= +nt
Spread
b
PC2 – 20.4%
PC1 – 31.5%
rpb1 A480S
rpb10 L25S
ssl1 I122T
tfb4 N71K
rad3 K499E
tfb2 F189S
spt5 G814*
spn1 V199G
c
Spearman ρ
1.00
0.22
0.00
d
ΔTSS spread
-30.00
0.00
30.00
e
n=2829
ΔTSS spread

1005

1006 **Figure 9. STRIPE-seq analysis of novel mutants identifies three functional groups of**
1007 **initiation mutants based on shift of spread of TSS distribution. a.** Schematic of Δspread
1008 metric of analysis **b.** Principal component analysis of Δspread values of top 2829 genes across
1009 mutants plotted along the first two principal components displays three clusters for Δmedian, ①
1010 chromatin mutants *spt5* G814*, *spn1* V199G, ② *rpb1* A480S, *rpb10* L25S, *ssl1* I122T, *tfb4*
1011 N71K and ③ *rad3* K499E and *tfb2* F189S. **c.** Hierarchical clustering of Spearman correlation of
1012 Δspread values across mutants. **d.** Hierarchically clustered heatmap of Δspread values across
1013 top 2829 promoters of mutants. **e.** Box-plot analysis of Δspread values across mutants
1014 presented by Tukey plot.

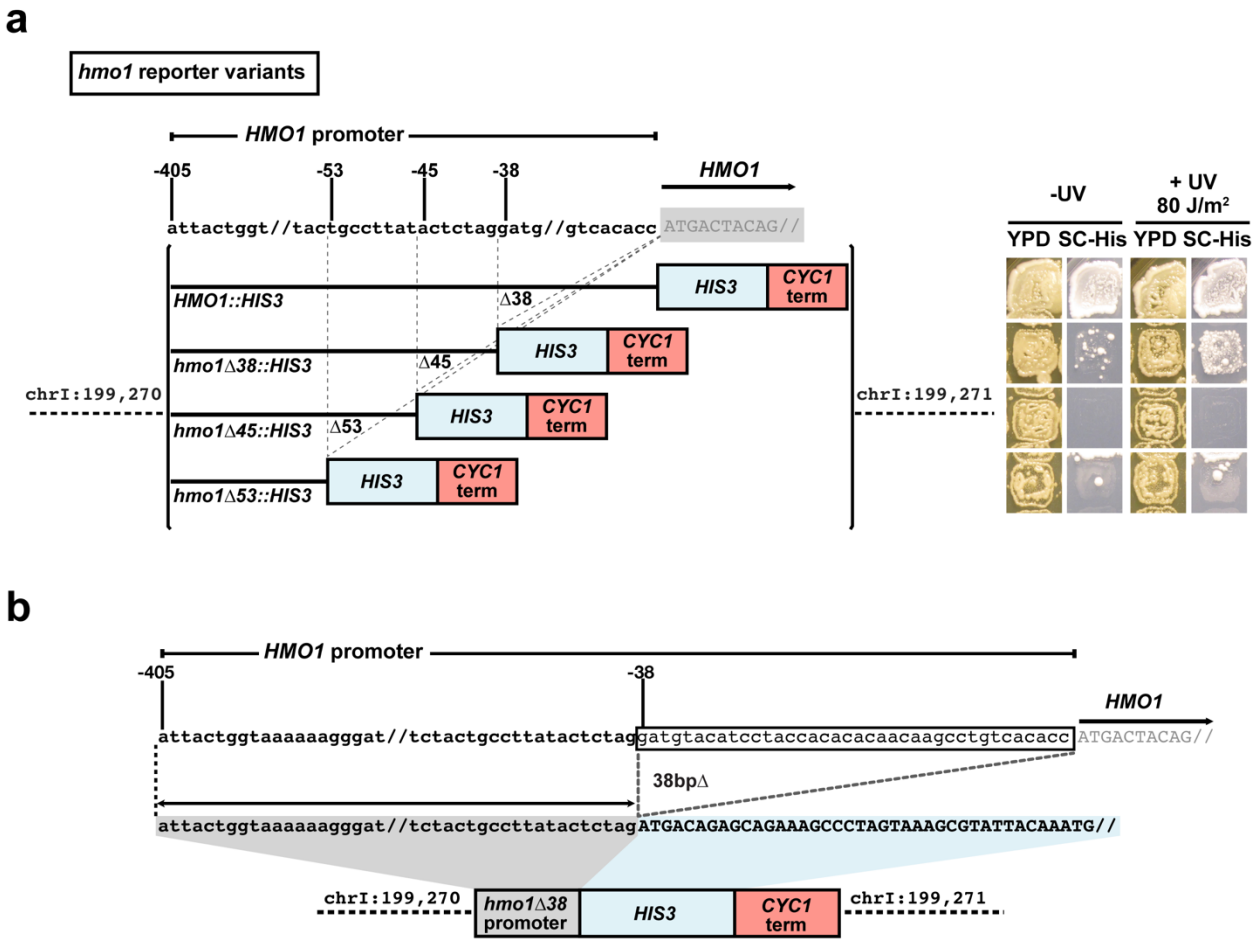

Figure S1. Isolation of *HMO1* promoter variant that detects upstream TSS shifts. a. Schematic illustrating an *HMO1* promoter variant deletion series (left) with behavior of reporters in cells in absence or presence of UV mutagenesis (right) to assess potential for His$^+$ mutant generation on the His$^-$ background, indicative of reporter suppression. **b.** Schematic of functional *hmo1Δ38::HIS3* reporter. *HMO1* promoter sequence between –405 and –39 was amplified and appended to the *HIS3* ORF followed by the *CYC1* terminator and integrated into a gene free region of chromosome I (chrI:199270-199271)**.**

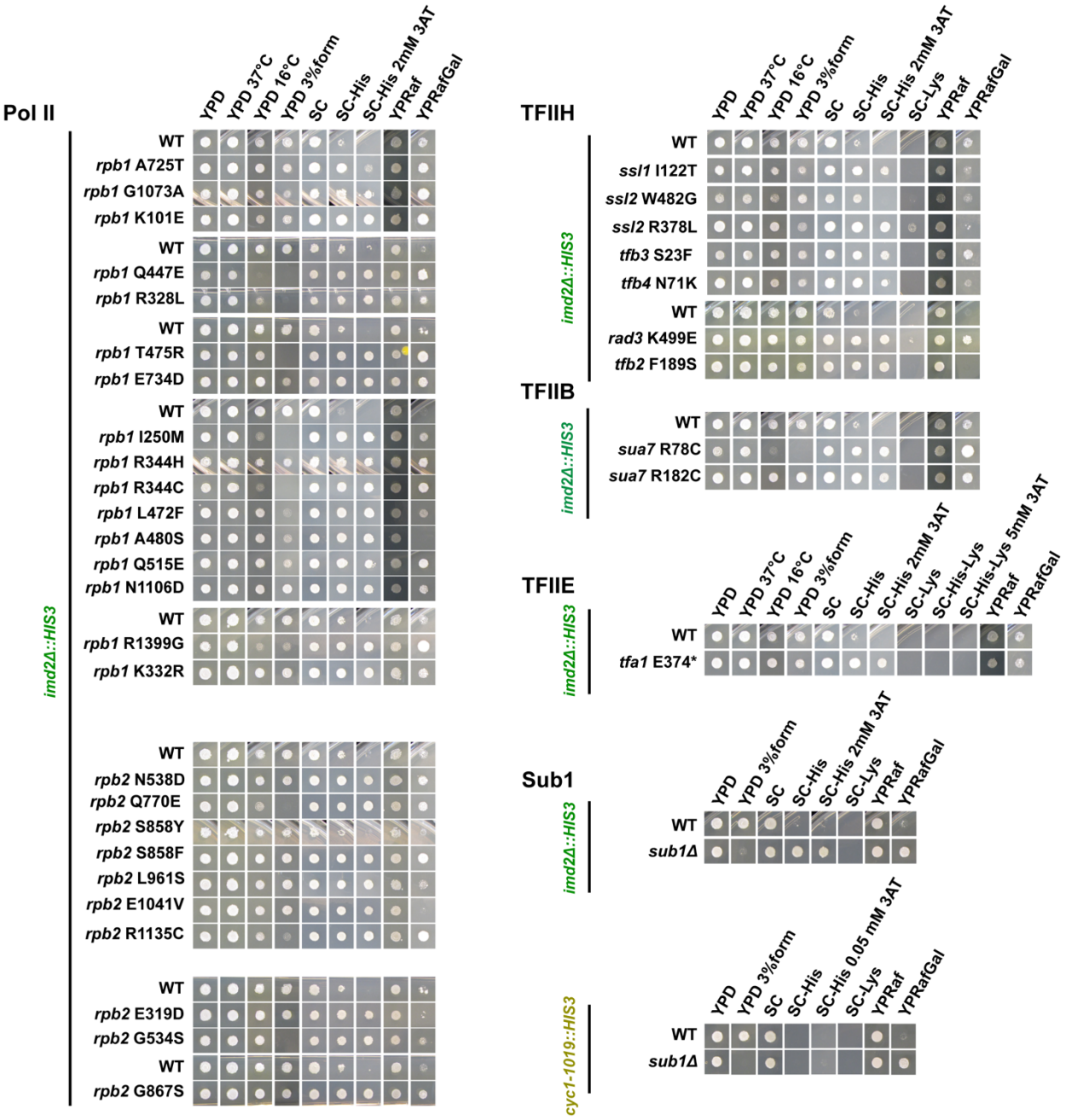

Figure S2. Initiation and secondary phenotypes of mutants isolated in genetic selections. Single spot phenotyping of a subset of downstream-shifting mutants isolated in our study.

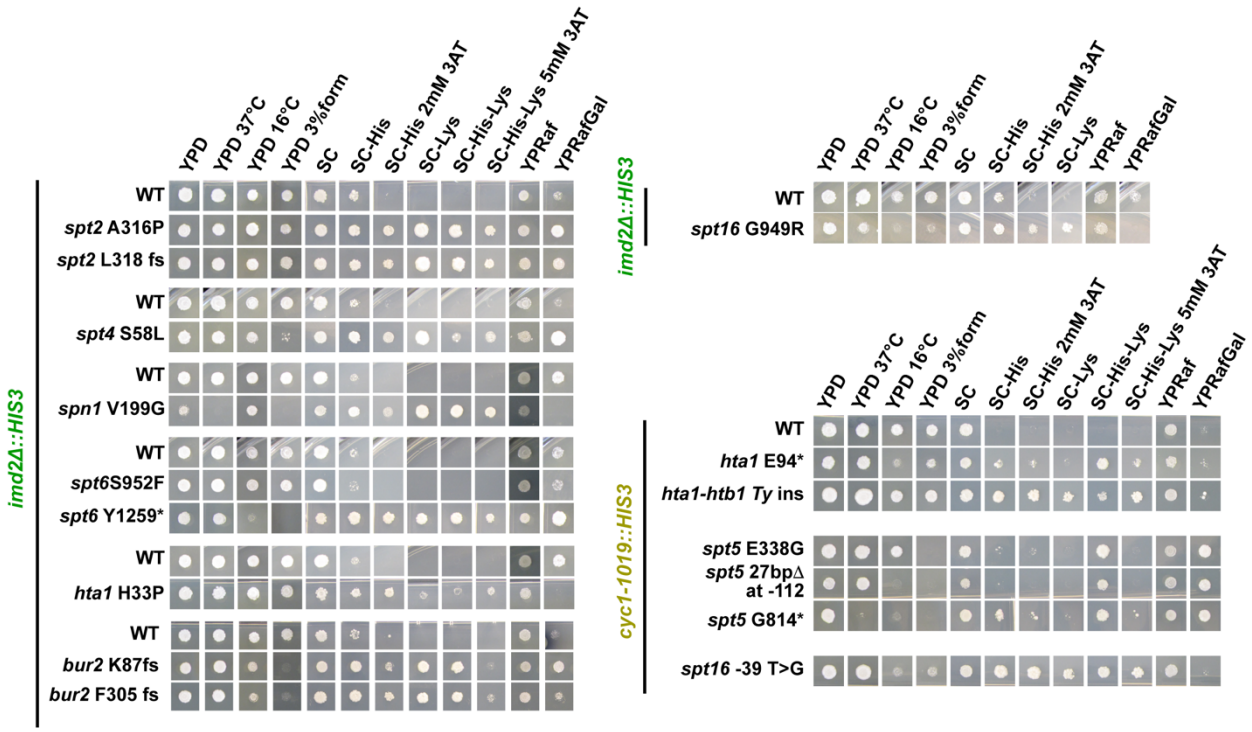

Figure S3. Phenotypes of chromatin mutants isolated in the study. Chromatin/Pol II elongation factor mutants identified for both downstream-shift sensitive reporters (subset shown).

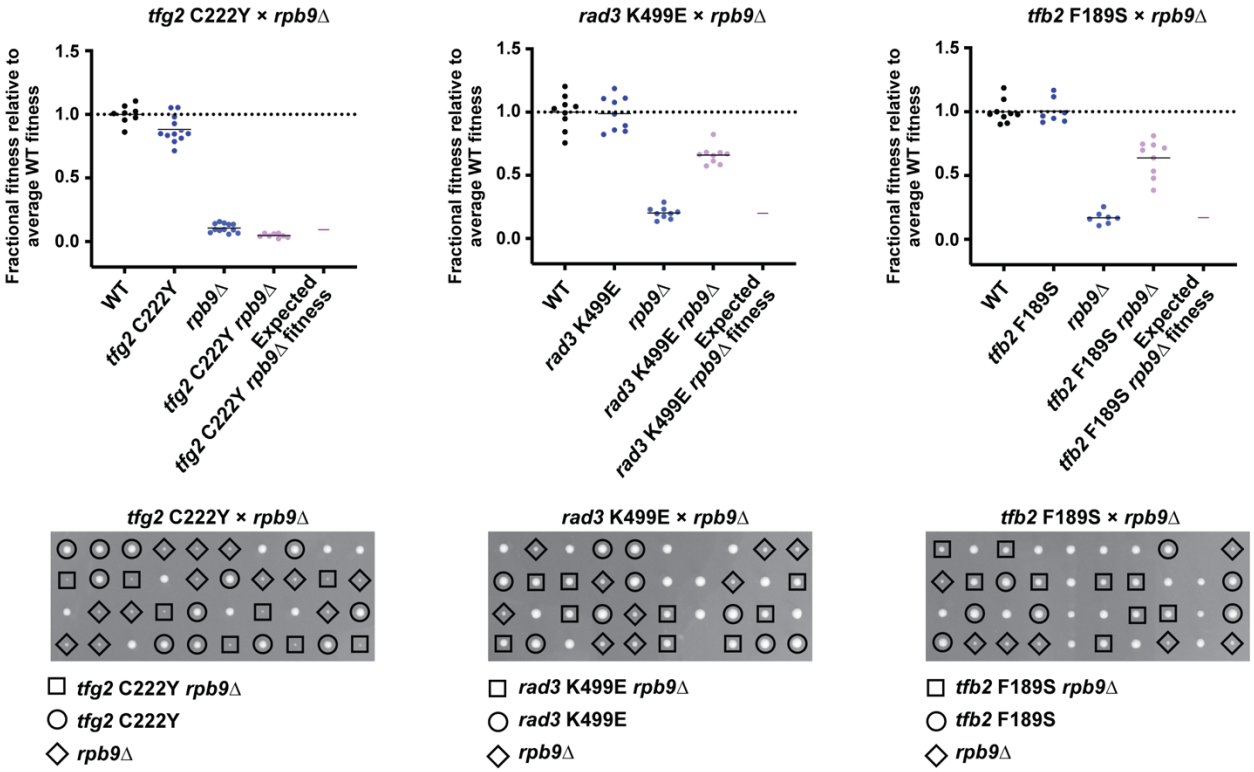

Figure S4. Genetic interactions between upstream-shifting *rpb9*Δ and subset of TFIIH downstream-shifting alleles. Left. Genetic interaction between *rpb9*Δ and *tfg2* C222Y. Growth phenotypes quantified through spore colony size as in Figure 6. **Middle-Right.** Suppression of *rpb9*Δ fitness defect by *rad3* K499E or *tfb2* F189S. Growth phenotypes quantified as above.

1035

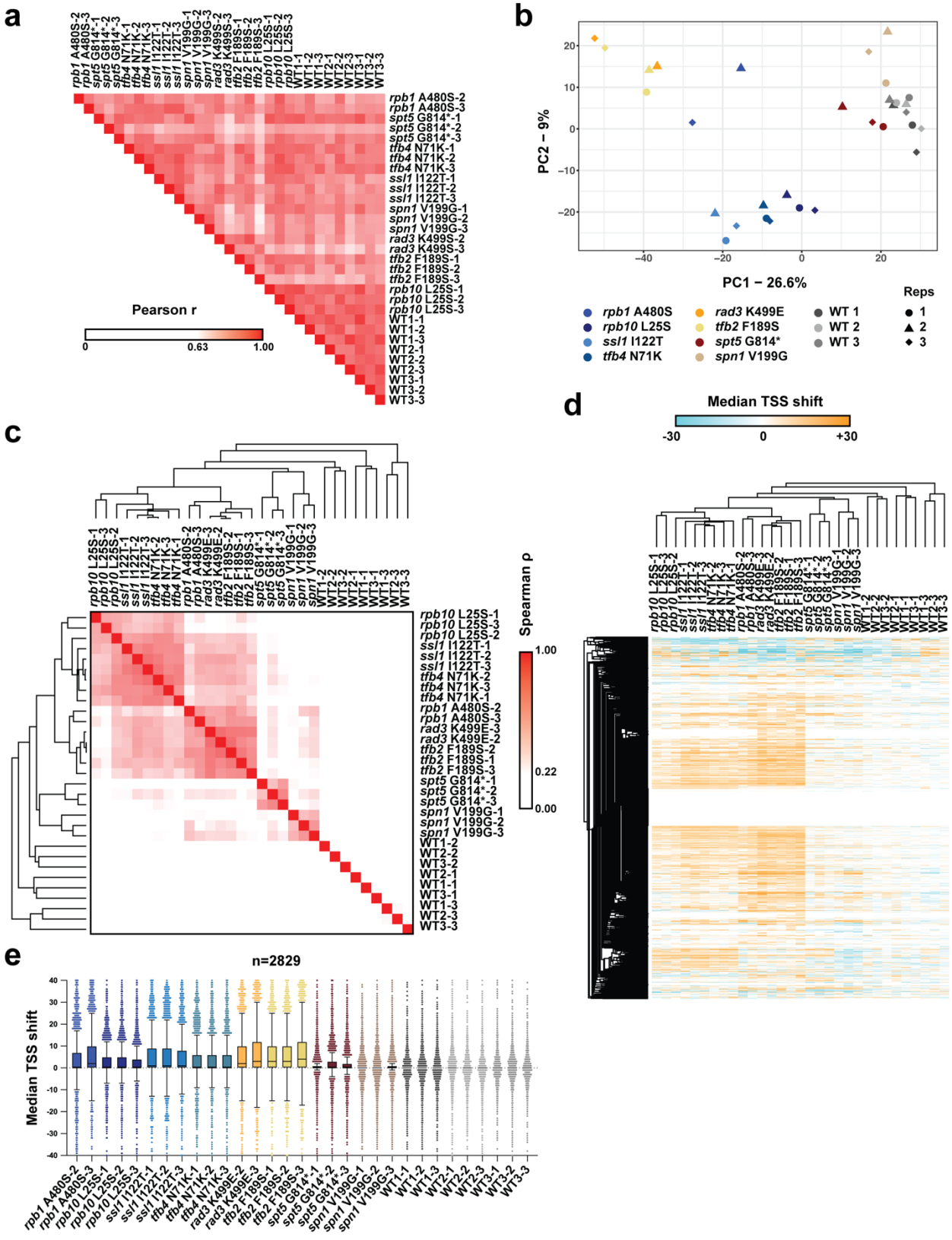
a
Pearson r
0
0.63
1.00
b
PC2 – 9%
PC1 – 26.6%
Reps
rpb1 A480S
rpb10 L25S
ssl1 I122T
tfb4 N71K
rad3 K499E
tfb2 F189S
spt5 G814*
spn1 V199G
WT 1
WT 2
WT 3
1
2
3
c
Spearman ρ
1.00
0.22
0.00
d
Median TSS shift
-30
0
+30
e
n=2829
Median TSS shift

1036

1037 **Figure S5. STRIPE-seq analysis of Δmedian values across individual mutant replicates. a.**
1038 Pearson correlation of individual TSS positions between samples across genome with cutoff per
1039 position set at ≥ 3. **b.** Principal component analysis of Δmedian values across top 2829 genes
1040 qualifying expression cutoff of ≥10 total expression within 401 base analyzed promoter window
1041 for individual sample replicates. **c.** Spearman correlation of Δmedian of top 2829 genes across
1042 all samples and replicates. **d.** Hierarchically clustered heatmap of Δmedian values across all
1043 promoters in individually sequenced samples. **e.** Box-plot analysis of these Δmedian values
1044 amongst all sequenced samples analyzed by Tukey's method.

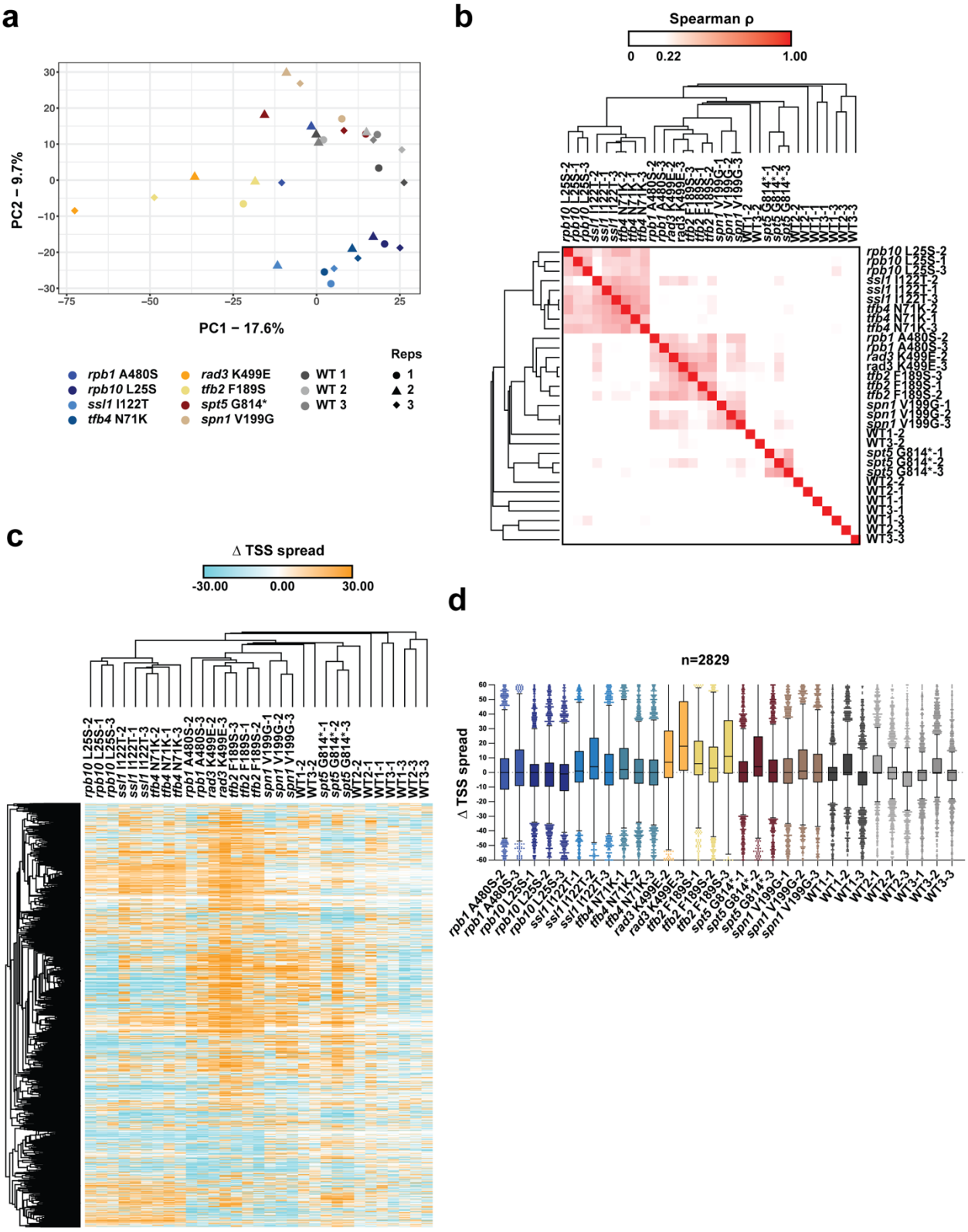

Figure S6. STRIPE-seq analysis of Δspread values across individual mutant replicates. a. Principal component analysis of Δspread values across top 2829 genes qualifying expression cutoff of ≥10 within 401 base analyzed promoter window for individual sample replicates. **b.**

1049 Pearson correlation of Δspread of top 2829 genes across all samples and replicates. **c.**
1050 Hierarchically clustered heatmap of Δspread values across all promoters in individually
1051 sequenced samples **d.** Box-plot analysis of these Δspread values amongst all sequenced
1052 samples analyzed by Tukey's method.

1053 **REFERENCES**

1054

1055 Picard Toolkit 2019. Broad Institute, Broad Institute, GitHub Repository.
1056 https://broadinstitute.github.io/picard/.
1057 Aibara, S., S. Schilbach and P. Cramer, 2021 Structures of mammalian RNA polymerase II pre-
1058 initiation complexes. Nature 594**:** 124-128.
1059 Amberg, D. C., D. J. Burke and J. N. Strathern, 2005 Methods in Yeast Genetics: A Cold Spring
1060 Harbor Laboratory Course Manual. Cold Spring Harbor, NY: Cold Spring Harbor
1061 PressCold Spring Harbor, NY: Cold Spring Harbor Press.
1062 Arribere, J. A., and W. V. Gilbert, 2013 Roles for transcript leaders in translation and mRNA
1063 decay revealed by transcript leader sequencing. Genome Res 23**:** 977-987.
1064 Baek, I., L. J. Friedman, J. Gelles and S. Buratowski, 2021 Single-molecule studies reveal
1065 branched pathways for activator-dependent assembly of RNA polymerase II pre-initiation
1066 complexes. Mol Cell 81**:** 3576-3588 e3576.
1067 Bangur, C. S., T. S. Pardee and A. S. Ponticelli, 1997 Mutational analysis of the D1/E1 core
1068 helices and the conserved N-terminal region of yeast transcription factor IIB (TFIIB):
1069 identification of an N-terminal mutant that stabilizes TATA-binding protein-TFIIB-DNA
1070 complexes. Mol Cell Biol 17**:** 6784-6793.
1071 Berroteran, R. W., D. E. Ware and M. Hampsey, 1994 The sua8 suppressors of Saccharomyces
1072 cerevisiae encode replacements of conserved residues within the largest subunit of RNA
1073 polymerase II and affect transcription start site selection similarly to sua7 (TFIIB)
1074 mutations. Mol Cell Biol 14**:** 226-237.
1075 Bolger, A. M., M. Lohse and B. Usadel, 2014 Trimmomatic: a flexible trimmer for Illumina
1076 sequence data. Bioinformatics 30**:** 2114-2120.
1077 Braberg, H., H. Jin, E. A. Moehle, Y. A. Chan, S. Wang *et al.*, 2013 From structure to systems:
1078 high-resolution, quantitative genetic analysis of RNA polymerase II. Cell 154**:** 775-788.
1079 Breathnach, R., and P. Chambon, 1981 Organization and expression of eucaryotic split genes
1080 coding for proteins. Annu Rev Biochem 50**:** 349-383.
1081 Brow, D. A., 2019 An Allosteric Network for Spliceosome Activation Revealed by High-
1082 Throughput Suppressor Analysis in Saccharomyces cerevisiae. Genetics 212**:** 111-124.
1083 Buratowski, S., S. Hahn, P. A. Sharp and L. Guarente, 1988 Function of a yeast TATA element-
1084 binding protein in a mammalian transcription system. Nature 334**:** 37-42.
1085 Cabart, P., H. Jin, L. Li and C. D. Kaplan, 2014 Activation and reactivation of the RNA
1086 polymerase II trigger loop for intrinsic RNA cleavage and catalysis. Transcription 5**:**
1087 e28869.
1088 Chen, B. S., and M. Hampsey, 2004 Functional interaction between TFIIB and the Rpb2 subunit
1089 of RNA polymerase II: implications for the mechanism of transcription initiation. Mol Cell
1090 Biol 24**:** 3983-3991.
1091 Chen, H. T., L. Warfield and S. Hahn, 2007 The positions of TFIIF and TFIIE in the RNA
1092 polymerase II transcription preinitiation complex. Nat Struct Mol Biol 14**:** 696-703.
1093 Cheung, V., G. Chua, N. N. Batada, C. R. Landry, S. W. Michnick *et al.*, 2008 Chromatin- and
1094 transcription-related factors repress transcription from within coding regions throughout
1095 the Saccharomyces cerevisiae genome. PLoS Biol 6**:** e277.
1096 Chu, Y., R. Simic, M. H. Warner, K. M. Arndt and G. Prelich, 2007 Regulation of histone
1097 modification and cryptic transcription by the Bur1 and Paf1 complexes. EMBO J 26**:**
1098 4646-4656.
1099 Cingolani, P., A. Platts, L. Wang le, M. Coon, T. Nguyen *et al.*, 2012 A program for annotating
1100 and predicting the effects of single nucleotide polymorphisms, SnpEff: SNPs in the
1101 genome of Drosophila melanogaster strain w1118; iso-2; iso-3. Fly (Austin) 6**:** 80-92.

1102 Clark-Adams, C. D., D. Norris, M. A. Osley, J. S. Fassler and F. Winston, 1988 Changes in
1103 histone gene dosage alter transcription in yeast. Genes Dev 2**:** 150-159.
1104 Clark-Adams, C. D., and F. Winston, 1987 The SPT6 gene is essential for growth and is
1105 required for delta-mediated transcription in Saccharomyces cerevisiae. Mol Cell Biol 7**:**
1106 679-686.
1107 Coin, F., J. C. Marinoni, C. Rodolfo, S. Fribourg, A. M. Pedrini *et al.*, 1998 Mutations in the XPD
1108 helicase gene result in XP and TTD phenotypes, preventing interaction between XPD
1109 and the p44 subunit of TFIIH. Nat Genet 20**:** 184-188.
1110 Conaway, R. C., and J. W. Conaway, 1993 General initiation factors for RNA polymerase II.
1111 Annu Rev Biochem 62**:** 161-190.
1112 Connell, Z., T. J. Parnell, L. L. McCullough, C. P. Hill and T. Formosa, 2022 The interaction
1113 between the Spt6-tSH2 domain and Rpb1 affects multiple functions of RNA Polymerase
1114 II. Nucleic Acids Res 50**:** 784-802.
1115 Cramer, P., D. A. Bushnell and R. D. Kornberg, 2001 Structural basis of transcription: RNA
1116 polymerase II at 2.8 angstrom resolution. Science 292**:** 1863-1876.
1117 Cui, P., H. Jin, M. R. Vutukuru and C. D. Kaplan, 2016 Relationships Between RNA Polymerase
1118 II Activity and Spt Elongation Factors to Spt- Phenotype and Growth in Saccharomyces
1119 cerevisiae. G3 (Bethesda) 6**:** 2489-2504.
1120 Danecek, P., A. Auton, G. Abecasis, C. A. Albers, E. Banks *et al.*, 2011 The variant call format
1121 and VCFtools. Bioinformatics 27**:** 2156-2158.
1122 Danecek, P., J. K. Bonfield, J. Liddle, J. Marshall, V. Ohan *et al.*, 2021 Twelve years of
1123 SAMtools and BCFtools. GigaScience 10.
1124 Davis, C. A., and M. Ares, Jr., 2006 Accumulation of unstable promoter-associated transcripts
1125 upon loss of the nuclear exosome subunit Rrp6p in Saccharomyces cerevisiae. Proc
1126 Natl Acad Sci U S A 103**:** 3262-3267.
1127 Deatherage, D. E., and J. E. Barrick, 2014 Identification of mutations in laboratory-evolved
1128 microbes from next-generation sequencing data using breseq. Methods Mol Biol 1151**:**
1129 165-188.
1130 Dobin, A., C. A. Davis, F. Schlesinger, J. Drenkow, C. Zaleski *et al.*, 2013 STAR: ultrafast
1131 universal RNA-seq aligner. Bioinformatics 29**:** 15-21.
1132 Doris, S. M., J. Chuang, O. Viktorovskaya, M. Murawska, D. Spatt *et al.*, 2018 Spt6 Is Required
1133 for the Fidelity of Promoter Selection. Mol Cell 72**:** 687-699 e686.
1134 Dudnyk, K., D. Cai, C. Shi, J. Xu and J. Zhou, 2024 Sequence basis of transcription initiation in
1135 the human genome. Science 384**:** eadj0116.
1136 Durr, G., J. Strayle, R. Plemper, S. Elbs, S. K. Klee *et al.*, 1998 The medial-Golgi ion pump
1137 Pmr1 supplies the yeast secretory pathway with Ca2+ and Mn2+ required for
1138 glycosylation, sorting, and endoplasmic reticulum-associated protein degradation. Mol
1139 Biol Cell 9**:** 1149-1162.
1140 Eichner, J., H. T. Chen, L. Warfield and S. Hahn, 2010 Position of the general transcription
1141 factor TFIIF within the RNA polymerase II transcription preinitiation complex. EMBO J
1142 29**:** 706-716.
1143 Ellison, M. A., J. L. Walker, P. J. Ropp, J. D. Durrant and K. M. Arndt, 2020 MutantHuntWGS: A
1144 Pipeline for Identifying Saccharomyces cerevisiae Mutations. G3 (Bethesda) 10**:** 3009-
1145 3014.
1146 Faitar, S. L., S. A. Brodie and A. S. Ponticelli, 2001 Promoter-specific shifts in transcription
1147 initiation conferred by yeast TFIIB mutations are determined by the sequence in the
1148 immediate vicinity of the start sites. Mol Cell Biol 21**:** 4427-4440.
1149 Fazal, F. M., C. A. Meng, K. Murakami, R. D. Kornberg and S. M. Block, 2015 Real-time
1150 observation of the initiation of RNA polymerase II transcription. Nature 525**:** 274-277.

1151 Fischbeck, J. A., S. M. Kraemer and L. A. Stargell, 2002 SPN1, a conserved gene identified by
1152 suppression of a postrecruitment-defective yeast TATA-binding protein mutant. Genetics
1153 162: 1605-1616.
1154 Fishburn, J., E. Tomko, E. Galburt and S. Hahn, 2015 Double-stranded DNA translocase activity
1155 of transcription factor TFIIH and the mechanism of RNA polymerase II open complex
1156 formation. Proc Natl Acad Sci U S A 112: 3961-3966.
1157 Freire-Picos, M. A., S. Krishnamurthy, Z. W. Sun and M. Hampsey, 2005 Evidence that the
1158 Tfg1/Tfg2 dimer interface of TFIIF lies near the active center of the RNA polymerase II
1159 initiation complex. Nucleic Acids Res 33: 5045-5052.
1160 Furter-Graves, E. M., R. Furter and B. D. Hall, 1991 SHI, a new yeast gene affecting the
1161 spacing between TATA and transcription initiation sites. Mol Cell Biol 11: 4121-4127.
1162 Furter-Graves, E. M., and B. D. Hall, 1990 DNA sequence elements required for transcription
1163 initiation of the Schizosaccharomyces pombe ADH gene in Saccharomyces cerevisiae.
1164 Mol Gen Genet 223: 407-416.
1165 Ghazy, M. A., S. A. Brodie, M. L. Ammerman, L. M. Ziegler and A. S. Ponticelli, 2004 Amino
1166 acid substitutions in yeast TFIIF confer upstream shifts in transcription initiation and
1167 altered interaction with RNA polymerase II. Mol Cell Biol 24: 10975-10985.
1168 Giardina, C., and J. T. Lis, 1993 DNA melting on yeast RNA polymerase II promoters. Science
1169 261: 759-762.
1170 Greger, I. H., A. Aranda and N. Proudfoot, 2000 Balancing transcriptional interference and
1171 initiation on the GAL7 promoter of Saccharomyces cerevisiae. Proc Natl Acad Sci U S A
1172 97: 8415-8420.
1173 Greger, I. H., and N. J. Proudfoot, 1998 Poly(A) signals control both transcriptional termination
1174 and initiation between the tandem GAL10 and GAL7 genes of Saccharomyces
1175 cerevisiae. EMBO J 17: 4771-4779.
1176 Gruber, J. D., K. Vogel, G. Kalay and P. J. Wittkopp, 2012 Contrasting properties of gene-
1177 specific regulatory, coding, and copy number mutations in Saccharomyces cerevisiae:
1178 frequency, effects, and dominance. PLoS Genet 8: e1002497.
1179 Hampsey, M., 1991 A tester system for detecting each of the six base-pair substitutions in
1180 Saccharomyces cerevisiae by selecting for an essential cysteine in iso-1-cytochrome c.
1181 Genetics 128: 59-67.
1182 Hampsey, M., 2006 The Pol II initiation complex: finding a place to start. Nat Struct Mol Biol 13:
1183 564-566.
1184 He, Y., C. Yan, J. Fang, C. Inouye, R. Tjian *et al.*, 2016 Near-atomic resolution visualization of
1185 human transcription promoter opening. Nature 533: 359-365.
1186 Hekmatpanah, D. S., and R. A. Young, 1991 Mutations in a conserved region of RNA
1187 polymerase II influence the accuracy of mRNA start site selection. Mol Cell Biol 11:
1188 5781-5791.
1189 Hemming, S. A., D. B. Jansma, P. F. Macgregor, A. Goryachev, J. D. Friesen *et al.*, 2000 RNA
1190 polymerase II subunit Rpb9 regulates transcription elongation in vivo. J Biol Chem 275:
1191 35506-35511.
1192 Hull, M. W., K. McKune and N. A. Woychik, 1995 RNA polymerase II subunit RPB9 is required
1193 for accurate start site selection. Genes Dev 9: 481-490.
1194 Hurowitz, E. H., and P. O. Brown, 2003 Genome-wide analysis of mRNA lengths in
1195 Saccharomyces cerevisiae. Genome Biol 5: R2.
1196 Janke, C., M. M. Magiera, N. Rathfelder, C. Taxis, S. Reber *et al.*, 2004 A versatile toolbox for
1197 PCR-based tagging of yeast genes: new fluorescent proteins, more markers and
1198 promoter substitution cassettes. Yeast 21: 947-962.
1199 Jenks, M. H., T. W. O'Rourke and D. Reines, 2008 Properties of an intergenic terminator and
1200 start site switch that regulate IMD2 transcription in yeast. Mol Cell Biol 28: 3883-3893.

1201 Jin, H., and C. D. Kaplan, 2014 Relationships of RNA polymerase II genetic interactors to
1202 transcription start site usage defects and growth in Saccharomyces cerevisiae. G3
1203 (Bethesda) 5: 21-33.
1204 Kadonaga, J. T., 1990 Assembly and disassembly of the Drosophila RNA polymerase II
1205 complex during transcription. J Biol Chem 265: 2624-2631.
1206 Kadonaga, J. T., 2012 Perspectives on the RNA polymerase II core promoter. Wiley Interdiscip
1207 Rev Dev Biol 1: 40-51.
1208 Kaplan, C. D., 2013 Basic mechanisms of RNA polymerase II activity and alteration of gene
1209 expression in Saccharomyces cerevisiae. Biochim Biophys Acta 1829: 39-54.
1210 Kaplan, C. D., M. J. Holland and F. Winston, 2005 Interaction between transcription elongation
1211 factors and mRNA 3'-end formation at the Saccharomyces cerevisiae GAL10-GAL7
1212 locus. J Biol Chem 280: 913-922.
1213 Kaplan, C. D., H. Jin, I. L. Zhang and A. Belyanin, 2012 Dissection of Pol II trigger loop function
1214 and Pol II activity-dependent control of start site selection in vivo. PLoS Genet 8:
1215 e1002627.
1216 Kaplan, C. D., L. Laprade and F. Winston, 2003 Transcription elongation factors repress
1217 transcription initiation from cryptic sites. Science 301: 1096-1099.
1218 Kaster, B. C., K. C. Knippa, C. D. Kaplan and D. O. Peterson, 2016 RNA Polymerase II Trigger
1219 Loop Mobility: INDIRECT EFFECTS OF Rpb9. J Biol Chem 291: 14883-14895.
1220 Khaperskyy, D. A., M. L. Ammerman, R. C. Majovski and A. S. Ponticelli, 2008 Functions of
1221 Saccharomyces cerevisiae TFIIF during transcription start site utilization. Mol Cell Biol
1222 28: 3757-3766.
1223 Kim, J. S., C. Saint-Andre, H. S. Lim, C. S. Hwang, J. M. Egly *et al.*, 2015 Crystal structure of
1224 the Rad3/XPD regulatory domain of Ssl1/p44. J Biol Chem 290: 8321-8330.
1225 Klopotowski, T., and A. Wiater, 1965 Synergism of aminotriazole and phosphate on the
1226 inhibition of yeast imidazole glycerol phosphate dehydratase. Arch Biochem Biophys
1227 112: 562-566.
1228 Knaus, R., R. Pollock and L. Guarente, 1996 Yeast SUB1 is a suppressor of TFIIB mutations
1229 and has homology to the human co-activator PC4. EMBO J 15: 1933-1940.
1230 Kopcewicz, K. A., T. W. O'Rourke and D. Reines, 2007 Metabolic regulation of IMD2
1231 transcription and an unusual DNA element that generates short transcripts. Mol Cell Biol
1232 27: 2821-2829.
1233 Kornberg, R. D., 2007 The molecular basis of eukaryotic transcription. Proc Natl Acad Sci U S A
1234 104: 12955-12961.
1235 Kostrewa, D., M. E. Zeller, K. J. Armache, M. Seizl, K. Leike *et al.*, 2009 RNA polymerase II-
1236 TFIIB structure and mechanism of transcription initiation. Nature 462: 323-330.
1237 Kubicek, C. E., R. D. Chisholm, S. Takayama and D. K. Hawley, 2013 RNA polymerase II
1238 mutations conferring defects in poly(A) site cleavage and termination in Saccharomyces
1239 cerevisiae. G3 (Bethesda) 3: 167-180.
1240 Kuehner, J. N., and D. A. Brow, 2006 Quantitative analysis of in vivo initiator selection by yeast
1241 RNA polymerase II supports a scanning model. J Biol Chem 281: 14119-14128.
1242 Kuehner, J. N., and D. A. Brow, 2008 Regulation of a eukaryotic gene by GTP-dependent start
1243 site selection and transcription attenuation. Mol Cell 31: 201-211.
1244 Langmead, B., and S. L. Salzberg, 2012 Fast gapped-read alignment with Bowtie 2. Nat
1245 Methods 9: 357-359.
1246 Laughery, M. F., T. Hunter, A. Brown, J. Hoopes, T. Ostbye *et al.*, 2015 New vectors for simple
1247 and streamlined CRISPR-Cas9 genome editing in Saccharomyces cerevisiae. Yeast 32:
1248 711-720.
1249 Li, H., B. Handsaker, A. Wysoker, T. Fennell, J. Ruan *et al.*, 2009 The Sequence
1250 Alignment/Map format and SAMtools. Bioinformatics 25: 2078-2079.

1251 Lifton, R. P., M. L. Goldberg, R. W. Karp and D. S. Hogness, 1978 The organization of the
1252 histone genes in Drosophila melanogaster: functional and evolutionary implications. Cold
1253 Spring Harb Symp Quant Biol 42 Pt 2: 1047-1051.
1254 Lin, Y. C., and J. D. Gralla, 2005 Stimulation of the XPB ATP-dependent helicase by the beta
1255 subunit of TFIIE. Nucleic Acids Res 33: 3072-3081.
1256 Lu, Z., and Z. Lin, 2019 Pervasive and dynamic transcription initiation in Saccharomyces
1257 cerevisiae. Genome Res 29: 1198-1210.
1258 Lu, Z., and Z. Lin, 2021 The origin and evolution of a distinct mechanism of transcription
1259 initiation in yeasts. Genome Res 31: 51-63.
1260 Luse, D. S., M. Parida, B. M. Spector, K. A. Nilson and D. H. Price, 2020 A unified view of the
1261 sequence and functional organization of the human RNA polymerase II promoter.
1262 Nucleic Acids Res 48: 7767-7785.
1263 Malabat, C., F. Feuerbach, L. Ma, C. Saveanu and A. Jacquier, 2015 Quality control of
1264 transcription start site selection by nonsense-mediated-mRNA decay. Elife 4.
1265 Malik, I., C. Qiu, T. Snavely and C. D. Kaplan, 2017 Wide-ranging and unexpected
1266 consequences of altered Pol II catalytic activity in vivo. Nucleic Acids Res 45: 4431-
1267 4451.
1268 Malone, E. A., C. D. Clark, A. Chiang and F. Winston, 1991 Mutations in SPT16/CDC68
1269 suppress cis- and trans-acting mutations that affect promoter function in Saccharomyces
1270 cerevisiae. Mol Cell Biol 11: 5710-5717.
1271 Mandal, D., T. B. Woolf and R. Rao, 2000 Manganese selectivity of pmr1, the yeast secretory
1272 pathway ion pump, is defined by residue gln783 in transmembrane segment 6. Residue
1273 Asp778 is essential for cation transport. J Biol Chem 275: 23933-23938.
1274 Mani, R., R. P. St Onge, J. L. t. Hartman, G. Giaever and F. P. Roth, 2008 Defining genetic
1275 interaction. Proc Natl Acad Sci U S A 105: 3461-3466.
1276 Martens, J. A., L. Laprade and F. Winston, 2004 Intergenic transcription is required to repress
1277 the Saccharomyces cerevisiae SER3 gene. Nature 429: 571-574.
1278 Martin, M., 2011 Cutadapt removes adapter sequences from high-throughput sequencing reads.
1279 EMBnet.journal 17.
1280 Miller, G., and S. Hahn, 2006 A DNA-tethered cleavage probe reveals the path for promoter
1281 DNA in the yeast preinitiation complex. Nat Struct Mol Biol 13: 603-610.
1282 Miura, F., N. Kawaguchi, J. Sese, A. Toyoda, M. Hattori *et al.*, 2006 A large-scale full-length
1283 cDNA analysis to explore the budding yeast transcriptome. Proc Natl Acad Sci U S A
1284 103: 17846-17851.
1285 Murakami, K., P. J. Mattei, R. E. Davis, H. Jin, C. D. Kaplan *et al.*, 2015 Uncoupling Promoter
1286 Opening from Start-Site Scanning. Mol Cell 59: 133-138.
1287 Na, J. G., I. Pinto and M. Hampsey, 1992 Isolation and characterization of SUA5, a novel gene
1288 required for normal growth in Saccharomyces cerevisiae. Genetics 131: 791-801.
1289 Nagalakshmi, U., Z. Wang, K. Waern, C. Shou, D. Raha *et al.*, 2008 The transcriptional
1290 landscape of the yeast genome defined by RNA sequencing. Science 320: 1344-1349.
1291 Niyogi, S. K., R. P. Feldman and D. J. Hoffman, 1981 Selective effects of metal ions on RNA
1292 synthesis rates. Toxicology 22: 9-21.
1293 Orphanides, G., T. Lagrange and D. Reinberg, 1996 The general transcription factors of RNA
1294 polymerase II. Genes Dev 10: 2657-2683.
1295 Pardee, T. S., C. S. Bangur and A. S. Ponticelli, 1998 The N-terminal region of yeast TFIIB
1296 contains two adjacent functional domains involved in stable RNA polymerase II binding
1297 and transcription start site selection. J Biol Chem 273: 17859-17864.
1298 Park, D., A. R. Morris, A. Battenhouse and V. R. Iyer, 2014 Simultaneous mapping of transcript
1299 ends at single-nucleotide resolution and identification of widespread promoter-
1300 associated non-coding RNA governed by TATA elements. Nucleic Acids Res 42: 3736-
1301 3749.

1302 Pelechano, V., W. Wei and L. M. Steinmetz, 2013 Extensive transcriptional heterogeneity
1303 revealed by isoform profiling. Nature 497: 127-131.
1304 Pinto, I., J. G. Na, F. Sherman and M. Hampsey, 1992a cis- and trans-acting suppressors of a
1305 translation initiation defect at the cyc1 locus of Saccharomyces cerevisiae. Genetics
1306 132: 97-112.
1307 Pinto, I., D. E. Ware and M. Hampsey, 1992b The yeast SUA7 gene encodes a homolog of
1308 human transcription factor TFIIB and is required for normal start site selection in vivo.
1309 Cell 68: 977-988.
1310 Pinto, I., W. H. Wu, J. G. Na and M. Hampsey, 1994 Characterization of sua7 mutations defines
1311 a domain of TFIIB involved in transcription start site selection in yeast. J Biol Chem 269:
1312 30569-30573.
1313 Policastro, R. A., D. J. McDonald, V. P. Brendel and G. E. Zentner, 2021 Flexible analysis of
1314 TSS mapping data and detection of TSS shifts with TSRexploreR. NAR Genom
1315 Bioinform 3: lqab051.
1316 Policastro, R. A., R. T. Raborn, V. P. Brendel and G. E. Zentner, 2020 Simple and efficient
1317 profiling of transcription initiation and transcript levels with STRIPE-seq. Genome Res
1318 30: 910-923.
1319 Policastro, R. A., and G. E. Zentner, 2022 Genome-Wide Profiling of Transcription Initiation with
1320 STRIPE-seq. Methods Mol Biol 2477: 21-34.
1321 Powers, E. N., C. Chan, E. Doron-Mandel, L. Llacsahuanga Allcca, J. Kim Kim *et al.*, 2022
1322 Bidirectional promoter activity from expression cassettes can drive off-target repression
1323 of neighboring gene translation. Elife 11.
1324 Prelich, G., and F. Winston, 1993 Mutations that suppress the deletion of an upstream activating
1325 sequence in yeast: involvement of a protein kinase and histone H3 in repressing
1326 transcription in vivo. Genetics 135: 665-676.
1327 Qiu, C., P. Arora, I. Malik, A. J. Laperuta, E. M. Pavlovic *et al.*, 2024 Thiolutin has complex
1328 effects in vivo but is a direct inhibitor of RNA polymerase II in vitro. Nucleic Acids Res
1329 52: 2546-2564.
1330 Qiu, C., O. C. Erinne, J. M. Dave, P. Cui, H. Jin *et al.*, 2016 High-Resolution Phenotypic
1331 Landscape of the RNA Polymerase II Trigger Loop. PLoS Genet 12: e1006321.
1332 Qiu, C., H. Jin, I. Vvedenskaya, J. A. Llenas, T. Zhao *et al.*, 2020 Universal promoter scanning
1333 by Pol II during transcription initiation in Saccharomyces cerevisiae. Genome Biol 21:
1334 132.
1335 Rando, O. J., and F. Winston, 2012 Chromatin and transcription in yeast. Genetics 190: 351-
1336 387.
1337 Rhee, H. S., and B. F. Pugh, 2012 Genome-wide structure and organization of eukaryotic pre-
1338 initiation complexes. Nature 483: 295-301.
1339 Roeder, R. G., 1996 The role of general initiation factors in transcription by RNA polymerase II.
1340 Trends Biochem Sci 21: 327-335.
1341 Roeder, R. G., 2019 50+ years of eukaryotic transcription: an expanding universe of factors and
1342 mechanisms. Nat Struct Mol Biol 26: 783-791.
1343 Rudolph, H. K., A. Antebi, G. R. Fink, C. M. Buckley, T. E. Dorman *et al.*, 1989 The yeast
1344 secretory pathway is perturbed by mutations in PMR1, a member of a Ca2+ ATPase
1345 family. Cell 58: 133-145.
1346 Sainsbury, S., J. Niesser and P. Cramer, 2013 Structure and function of the initially transcribing
1347 RNA polymerase II-TFIIB complex. Nature 493: 437-440.
1348 Sandelin, A., P. Carninci, B. Lenhard, J. Ponjavic, Y. Hayashizaki *et al.*, 2007 Mammalian RNA
1349 polymerase II core promoters: insights from genome-wide studies. Nat Rev Genet 8:
1350 424-436.

1351 Schilbach, S., S. Aibara, C. Dienemann, F. Grabbe and P. Cramer, 2021 Structure of RNA
1352 polymerase II pre-initiation complex at 2.9 A defines initial DNA opening. Cell 184: 4064-
1353 4072 e4028.
1354 Schilbach, S., M. Hantsche, D. Tegunov, C. Dienemann, C. Wigge *et al.*, 2017 Structures of
1355 transcription pre-initiation complex with TFIIH and Mediator. Nature 551: 204-209.
1356 Schmitt, M. E., T. A. Brown and B. L. Trumpower, 1990 A rapid and simple method for
1357 preparation of RNA from Saccharomyces cerevisiae. Nucleic Acids Res 18: 3091-3092.
1358 Sikorski, T. W., S. B. Ficarro, J. Holik, T. Kim, O. J. Rando *et al.*, 2011 Sub1 and RPA associate
1359 with RNA polymerase II at different stages of transcription. Mol Cell 44: 397-409.
1360 Simchen, G., F. Winston, C. A. Styles and G. R. Fink, 1984 Ty-mediated gene expression of the
1361 LYS2 and HIS4 genes of Saccharomyces cerevisiae is controlled by the same SPT
1362 genes. Proc Natl Acad Sci U S A 81: 2431-2434.
1363 Smale, S. T., and J. T. Kadonaga, 2003 The RNA polymerase II core promoter. Annu Rev
1364 Biochem 72: 449-479.
1365 Smith, T., A. Heger and I. Sudbery, 2017 UMI-tools: modeling sequencing errors in Unique
1366 Molecular Identifiers to improve quantification accuracy. Genome Res 27: 491-499.
1367 Struhl, K., 1987 Promoters, activator proteins, and the mechanism of transcriptional initiation in
1368 yeast. Cell 49: 295-297.
1369 Struhl, K., and R. W. Davis, 1977 Production of a functional eukaryotic enzyme in Escherichia
1370 coli: cloning and expression of the yeast structural gene for imidazole-glycerolphosphate
1371 dehydratase (his3). Proc Natl Acad Sci U S A 74: 5255-5259.
1372 Sun, Z. W., and M. Hampsey, 1995 Identification of the gene (SSU71/TFG1) encoding the
1373 largest subunit of transcription factor TFIIF as a suppressor of a TFIIB mutation in
1374 Saccharomyces cerevisiae. Proc Natl Acad Sci U S A 92: 3127-3131.
1375 Sun, Z. W., and M. Hampsey, 1996 Synthetic enhancement of a TFIIB defect by a mutation in
1376 SSU72, an essential yeast gene encoding a novel protein that affects transcription start
1377 site selection in vivo. Mol Cell Biol 16: 1557-1566.
1378 Sun, Z. W., A. Tessmer and M. Hampsey, 1996 Functional interaction between TFIIB and the
1379 Rpb9 (Ssu73) subunit of RNA polymerase II in Saccharomyces cerevisiae. Nucleic Acids
1380 Res 24: 2560-2566.
1381 Swanson, M. S., E. A. Malone and F. Winston, 1991 SPT5, an essential gene important for
1382 normal transcription in Saccharomyces cerevisiae, encodes an acidic nuclear protein
1383 with a carboxy-terminal repeat. Mol Cell Biol 11: 3009-3019.
1384 Tomko, E. J., J. Fishburn, S. Hahn and E. A. Galburt, 2017 TFIIH generates a six-base-pair
1385 open complex during RNAP II transcription initiation and start-site scanning. Nat Struct
1386 Mol Biol 24: 1139-1145.
1387 Tomko, E. J., O. Luyties, J. K. Rimel, C. L. Tsai, J. O. Fuss *et al.*, 2021 The Role of XPB/Ssl2
1388 dsDNA Translocase Processivity in Transcription Start-site Scanning. J Mol Biol 433:
1389 166813.
1390 Vaser, R., S. Adusumalli, S. N. Leng, M. Sikic and P. C. Ng, 2016 SIFT missense predictions for
1391 genomes. Nat Protoc 11: 1-9.
1392 Vo Ngoc, L., Y. L. Wang, G. A. Kassavetis and J. T. Kadonaga, 2017 The punctilious RNA
1393 polymerase II core promoter. Genes Dev 31: 1289-1301.
1394 Wang, M., P. Arora, C. D. Kaplan and D. A. Brow, 2025 Substitutions in RNA-binding protein
1395 Hrp1 map a potential interaction surface with the yeast RNA polymerase II elongation
1396 complex. Genetics.
1397 Winston, F., D. T. Chaleff, B. Valent and G. R. Fink, 1984 Mutations affecting Ty-mediated
1398 expression of the HIS4 gene of Saccharomyces cerevisiae. Genetics 107: 179-197.
1399 Woychik, N. A., W. S. Lane and R. A. Young, 1991 Yeast RNA polymerase II subunit RPB9 is
1400 essential for growth at temperature extremes. J Biol Chem 266: 19053-19055.

1401 Wu, W. H., I. Pinto, B. S. Chen and M. Hampsey, 1999 Mutational analysis of yeast TFIIB. A
1402 functional relationship between Ssu72 and Sub1/Tsp1 defined by allele-specific
1403 interactions with TFIIB. Genetics 153: 643-652.
1404 Xie, Y., H. Li, X. Luo, H. Li, Q. Gao *et al.*, 2022 IBS 2.0: an upgraded illustrator for the
1405 visualization of biological sequences. Nucleic Acids Res 50: W420-W426.
1406 Xu, Z., W. Wei, J. Gagneur, F. Perocchi, S. Clauder-Munster *et al.*, 2009 Bidirectional promoters
1407 generate pervasive transcription in yeast. Nature 457: 1033-1037.
1408 Yang, C., P. Basnet, S. Sharmin, H. Shen, C. D. Kaplan *et al.*, 2024 Transcription start site
1409 scanning requires the fungi-specific hydrophobic loop of Tfb3. Nucleic Acids Res 52:
1410 11602-11611.
1411 Yang, C., R. Fujiwara, H. J. Kim, P. Basnet, Y. Zhu *et al.*, 2022 Structural visualization of de
1412 novo transcription initiation by Saccharomyces cerevisiae RNA polymerase II. Mol Cell
1413 82: 660-676 e669.
1414 Yoon, H., S. P. Miller, E. K. Pabich and T. F. Donahue, 1992 SSL1, a suppressor of a HIS4 5'-
1415 UTR stem-loop mutation, is essential for translation initiation and affects UV resistance
1416 in yeast. Genes Dev 6: 2463-2477.
1417 Zhang, Z., and F. S. Dietrich, 2005 Mapping of transcription start sites in Saccharomyces
1418 cerevisiae using 5' SAGE. Nucleic Acids Res 33: 2838-2851.
1419 Zhao, T., I. O. Vvedenskaya, W. K. Lai, S. Basu, B. F. Pugh *et al.*, 2021 Ssl2/TFIIH function in
1420 transcription start site scanning by RNA polymerase II in Saccharomyces cerevisiae.
1421 Elife 10.
1422 Zhu, Y., I. O. Vvedenskaya, S. H. Sze, B. E. Nickels and C. D. Kaplan, 2024 Quantitative
1423 analysis of transcription start site selection reveals control by DNA sequence, RNA
1424 polymerase II activity and NTP levels. Nat Struct Mol Biol 31: 190-202.

1425